AD-A282 404 MICROMECHANICS OF INTERFACES IN METAL MATRIX COMPOSITES 1/1
(U) MINNESOTA UNIV MINNEAPOLIS W W GERBERICH ET AL.
12 JUL 94 XB-ONR N00014-92-J-1962
UNCLASSIFIED NL

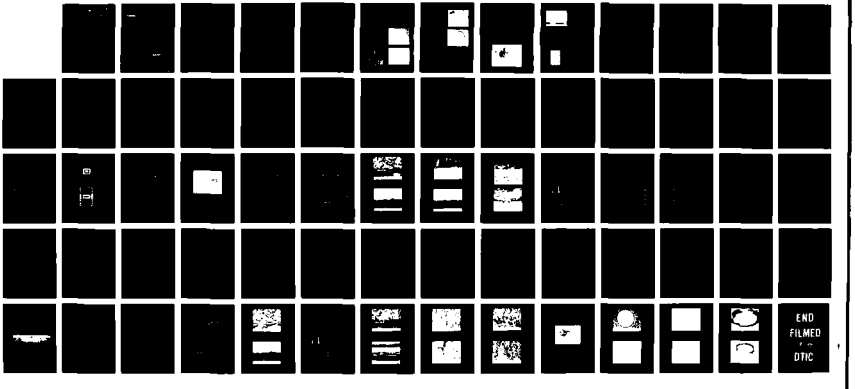

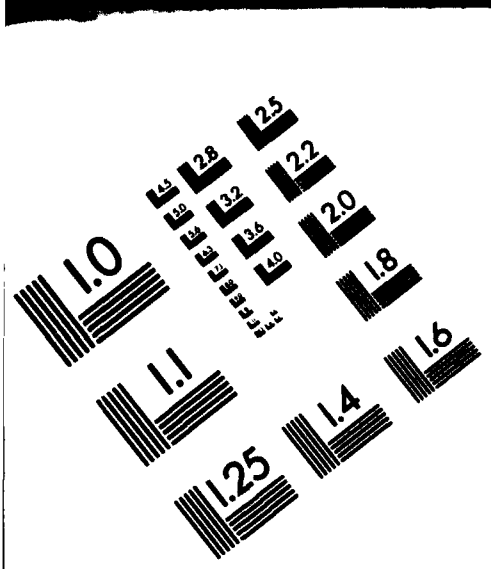

Association for Information and Image Management
1100 Wayne Avenue, Suite 1100
Silver Spring, Maryland 20910
301/587-8202

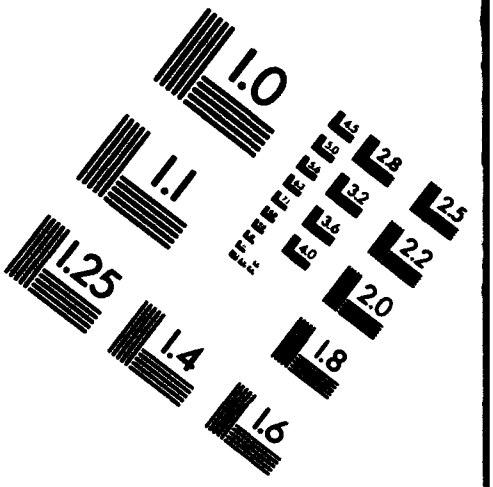

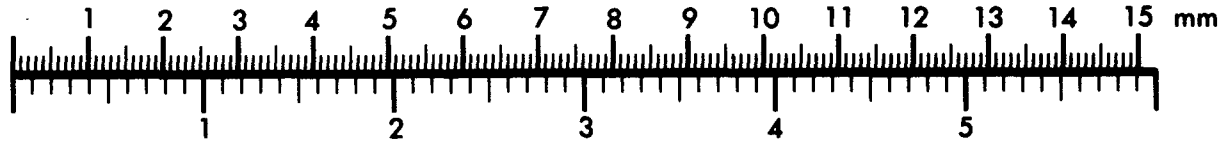

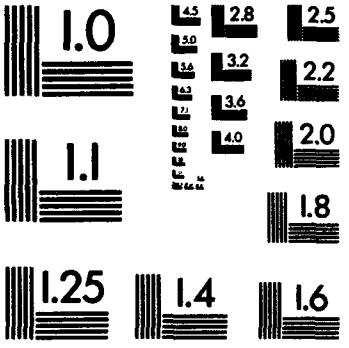

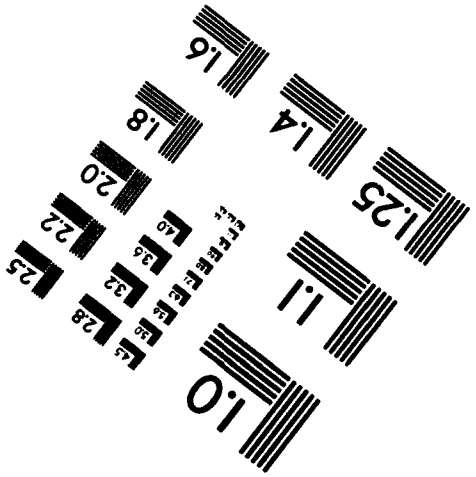

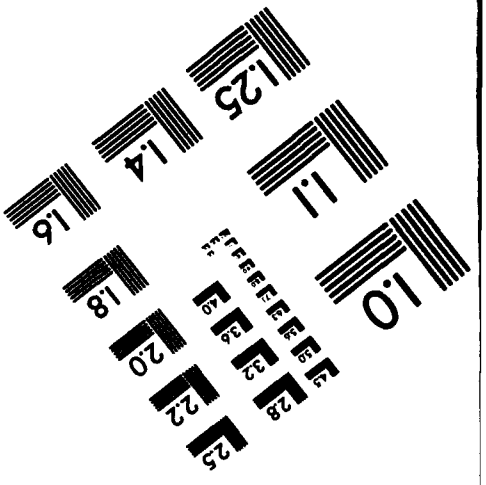

MANUFACTURED TO AIIM STANDARDS
BY APPLIED IMAGE, INC.

MICROMECHANICS OF INTERFACES IN METAL MATRIX COMPOSITES

FINAL TECHNICAL REPORT
July 12, 1994
Grant N00014-92-J-1962

submitted by:

Professor William W. Gerberich
Chemical Engineering and Materials Science

Professor David L. Kohlstedt
Geology and Geophysics
University of Minnesota
Minneapolis, MN 55455

submitted to:

Dr. Steven Fishman
Code 1131
Office of Naval Research
800 N. Quincy Street
Arlington, VA 22217

CONTENTS

A. INTRODUCTION

As was stated in the original statement of work, the proposed work was to (i) evaluate the interfacial fracture toughness of Ti/Al_2O_3 with and without a diffusion barrier, (ii) use various surface science techniques to evaluate these interfaces, (iii) explore the possibility of using fiber pushout techniques in Al_2O_3 fiber-reinforced titanium alloy composite, and (iv) compare the data from four-point bend and microscratch tests to calibrate the interfacial fracture toughness in the Ti/Al_2O_3 system.

These goals have been successfully met as outlined in the following three sections. In Part I, which has already been published, we demonstrate that interfacial shear strengths, as measured by fiber pushout, and fiber frictional characteristics, as measured by lateral force microscopy, can be utilized to understand the micromechanics of composite interfaces. This was the first successful attempt at pushing out 10 μm sized fibers by nanoindentation. This was followed up by a combined study of microscratch toughness and four-point bending of pre-crack laminates in an attempt to validate the microscratch technique. This turned out to be very successful as outlined in Part II with a correlation of toughness which extended over three decades of thickness. The significance of this is that interfacial barrier coatings and their effect on interfacial fracture toughness may be more easily studied with thin film prototypes as a screening test. Finally, in Part III, the comparison of four-point bend and fiber pushout characterization of Al_2O_3/Ti couples with and without barrier coatings is accomplished. Effects of process control temperature on interfacial chemistries and their impact on interfacial fracture energies are documented.

Interfacial stability and mechanical properties of Al_2O_3 fiber reinforced Ti matrix composites

Hsin-Fu Wang, John C. Nelson, Chien-Li Lin, and William W. Gerberich
Department of Chemical Engineering and Materials Science, University of Minnesota, Minneapolis, Minnesota 55455-0132

(Received 6 July 1993; accepted 21 September 1993)

The mechanical properties of the interfaces in an Al_2O_3 fiber reinforced β-21S Ti alloy have been evaluated by using fiber pushout tests. The Al_2O_3 fibers were coated with a refractory metal and Y_2O_3 which served as a diffusion barrier during the HIPing used to produce the metal matrix composites. By doing fiber pushout tests, the interfacial fracture was found to occur at the interface between the refractory metal and the Y_2O_3. The interfacial shear strength and interfacial frictional stress were measured to be 323 and 312 $\pm$ 2 MPa, respectively. The interfacial frictional stress, which is due to asperity interlocking during the fiber sliding, was correlated to the surface roughness of the coated Al_2O_3 fiber obtained with the aid of an atomic force microscope. The measured surface roughness of 18.8 $\pm$ 2.2 nm was related to the frictional stress through Hutchinson's model.[9] The frictional coefficient between the Al_2O_3 fiber and the Ti matrix is calculated to be 0.32 $\pm$ 0.02.

I. INTRODUCTION

Continuous fiber reinforced Ti matrix composites have received attention in the aerospace industry as advanced structural materials because of their high specific strength, excellent corrosion resistance, and good high temperature thermal stability.[1-3] The macroscopic mechanical properties of these composites are controlled not only by the mechanical properties of the constituents but also by the adhesion strength of the fiber/matrix interfaces. Because the fiber bridging effect reduces the stress intensity at the crack tip during crack propagation in composites, the interfacial mechanical properties, such as interfacial shear strength and interfacial frictional stress, have a dominant effect on the overall fracture toughness of the composites.[4,5] To measure the mechanical properties of the interfaces, fiber pushout tests have been widely used.[6-8] This method is relatively simple compared to the fiber pullout test and provides a simulation of the interfacial debonding and sliding between a fiber and the matrix that takes place in composites fracturing under mode I loading.

By doing the fiber pushout tests, the interfacial shear strength and interfacial frictional stress were obtained. Microstructural observation and chemical analysis of the composite after the pushout tests were performed by using a scanning electron microscope and x-ray mapping. This study also focuses on the evaluation of the surface roughness of the coated Al_2O_3 fibers by using an atomic force microscope (AFM). By using the measured surface roughness and fiber pushout test results in Hutchinson's model,[9] the friction coefficient can be calculated. As far as we know, this represents the first study of frictional effects based upon the pushout test of such very small diameter fibers (10 μm).

II. EXPERIMENTAL PROCEDURES

A. Instruments

1. The capacity of the continuous microindentation equipment

All of these experiments were performed by using a load and depth sensing indentation instrument with sensitivities in the nanoscale range. The indenter vertical displacement is controlled by using a stepper motor for coarse displacement on the order of microns. The fine displacement on the order of nanometers is controlled using a piezoelectric transducer (PZT). The PZT can control the indenter with a depth resolution of 0.5 nm, while the load cell has a capacity of 0.9 N and a load resolution of 16 μN.

2. Atomic force microscope

In the AFM studies, a Digital Nanoscope III System was used to perform the measurement of the surface roughness on the refractory metal/Y_2O_3 coated fiber in air. A force sensor, consisting of a Si_3N_4 cantilever with radius of curvature about 40 nm, produced lateral and vertical resolutions of 2 nm and 1 Å, respectively. Each image consists of 256 lines of 256 points.

B. Fiber pushout tests

1. Sample preparation

The composites used in this test were provided by 3M Company. For the reinforcement, 10 μm Al_2O_3 fibers were made from a sol-gel process (purity 99.5%). The fibers were coated with a refractory metal and Y_2O_3 duplex coating, the nature of which is proprietary, to reduce the chemical reaction between the fiber and the matrix. The composite was prepared by using hot isostatic press diffusion bonding of the fibers and β-21S Ti alloy at 900 °C.

A sample with thickness of around 0.3 mm was cut perpendicular to the Al_2O_3 fibers by using a low speed diamond saw. This was thinned down to 100 μm by sanding followed by polishing with 1.0 μm diamond paste. A final thinning and polishing was performed using a dimpler with a sample thickness monitor. The thickness of the specimen for the fiber pushout test was 30 $\pm$ 0.5 μm. This was measured accurately by using a scanning electron microscope. The specimen was set on a supporting block made of Al 2024 alloy with a slot 50 μm deep and 200 μm wide. This slot allows the pushed-out fibers to be traction-free at the pushout end. A thin layer of wax was carefully coated at the edge of the slot to fix the specimens for the tests. The specimen was set carefully to make sure that the thinned area was sitting on the top of the slot.

2. Testing procedures

The schematic diagram of the setup for the fiber pushout tests is shown in Fig. 1. The fiber pushout tests were performed by driving a flat tip indenter into the fiber. During the test, the load-displacement curve was recorded continuously by using an IBM personal computer and a chart recorder. When the displacement of the fiber was about 3 μm, the indenter was unloaded. The load-displacement data were used to calculate the interfacial shear strength and interfacial frictional stress. Scanning electron microscopy and x-ray mapping were performed to analyze the fracture surface after the pushout test.

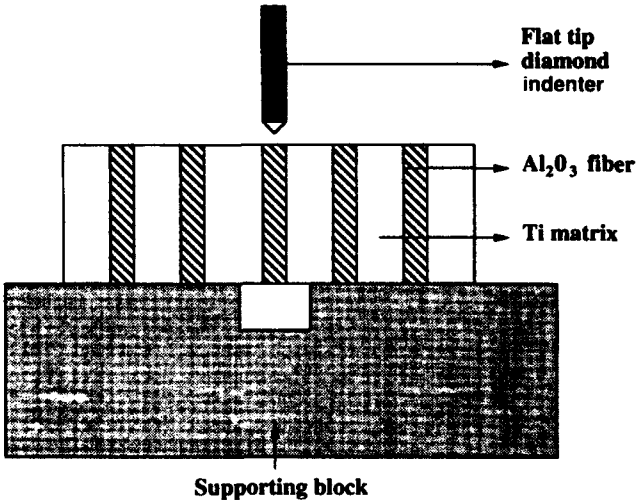

FIG. 1. Schematic diagram of the setup for the fiber pushout tests.

III. RESULTS AND DISCUSSION

A. Fiber pushout tests

1. Observation and analysis of interfacial failure

A SEM micrograph of the Al_2O_3 fiber reinforced Ti matrix composite is shown in Fig. 2(a), and the x-ray mapping of this composite is shown in Fig. 2(b). It is seen that some Al has diffused across the Y_2O_3

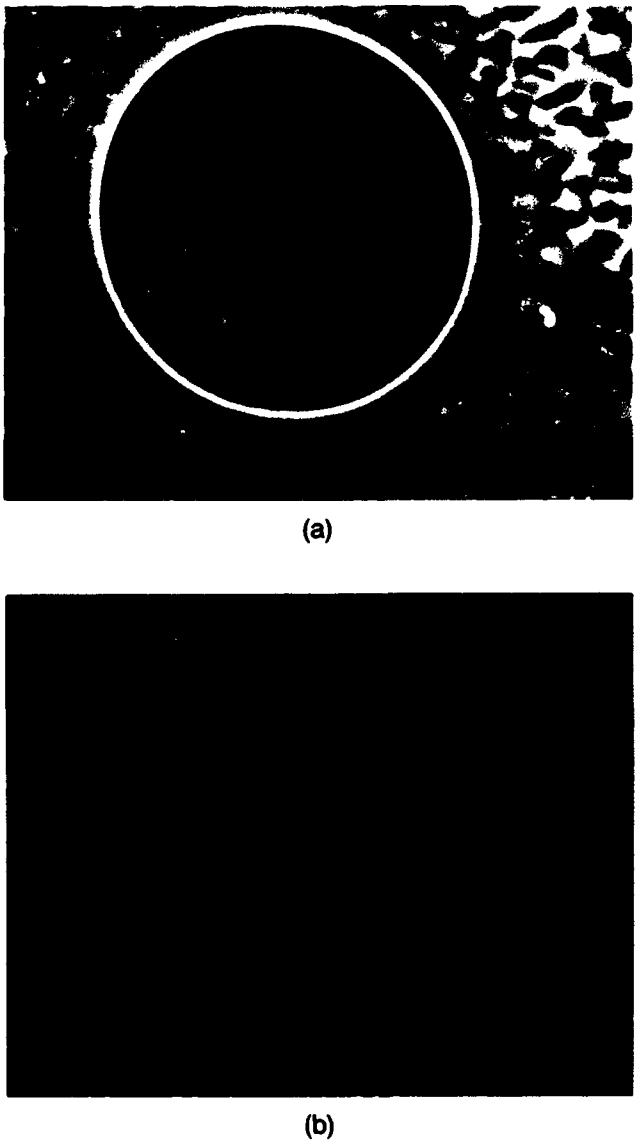

FIG. 2. SEM micrograph and x-ray mapping of the fiber composite. (a) SEI image. (b) Aluminum x-ray mapping.

and the refractory metal diffusion barrier and into the β-21S Ti matrix to a distance of about 0.7 μm. The purpose of the diffusion barrier is to prevent the diffusion of Al into Ti during the HIPing process. It will form a Ti_3Al intermetallic compound that will degrade the fracture toughness of the composite.[10] The effect of the diffusion barrier is exhibited by noting that under similar processing conditions the diffusion distance of Al into Ti without the diffusion barrier is about 5 μm.[10] The load-displacement curve of a fiber pushout test is shown in Fig. 3. At first, the load increased with increasing displacement. This corresponds to the initial elastic loading. There is a load drop at 0.3 N, which means that the initial debonding between the fiber and the matrix occurred. Then, debonding and fiber sliding continued concurrently to a fiber sliding distance of 1 μm, which marked the end of debonding. After the fiber had slid another 1.5 μm, the unloading stage was initiated. A fiber after the pushout test is shown in Fig. 4. From x-ray mapping, it is clear that the interfacial fracture process occurred between the refractory metal and the Y_2O_3 interface. Parallel experiments using the same Al_2O_3 fiber reinforced Ti composite in a tensile test show some fiber pullout. The x-ray mapping of those fibers confirms that interfacial fracture also occurred at the interface between the refractory metal and the Y_2O_3. This gives additional support for the use of the fiber pushout test as a simulation of the interfacial debonding and sliding event that happens in fiber composites under tensile loading.[11,12]

2. Calculation of interfacial adhesion strength

The interfacial shear strength (τ_i) and interfacial frictional stress (τ) were calculated as follows:

$$\tau_i = \frac{P_{cr}}{2\pi Rt} \quad (1)$$

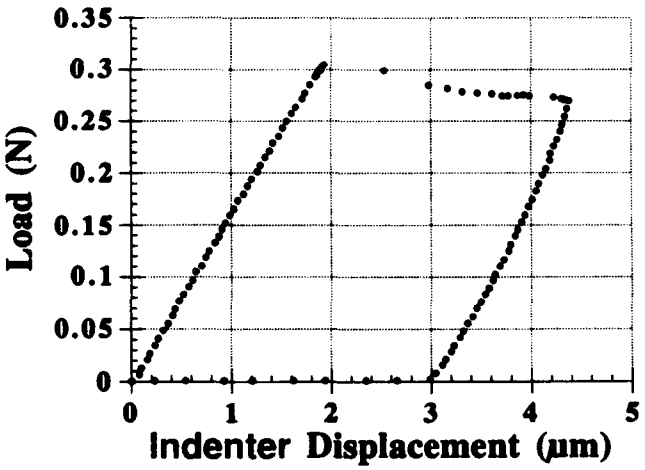

FIG. 3. The load-displacement curve for the fiber pushout test.

(a)

(b)

FIG. 4. The morphology of the fiber composite after the pushout test. (a) The indented fiber. (b) The pushed-out fiber.

$$\tau = \frac{P}{2\pi R(t - d)} \quad (2)$$

where P_{cr} is the critical load measured from the pushout test, R is the radius of the fiber, t is the thickness of the composite, and d is the pushout length of the fiber. The relationship between the interfacial frictional stress and fiber displacement is shown in Fig. 5. The calculated interfacial shear strength and interfacial frictional stress are 323 MPa and 312 $\pm$ 2 MPa, respectively. The calculated interfacial shear strength is a little higher than that of a boron fiber reinforced Ti-6-4 alloy composite which is 275 MPa.[3]

B. Atomic force microscopy study

An AFM image of the as-received coated Al_2O_3 fiber is shown in Fig. 6. The surface features of the

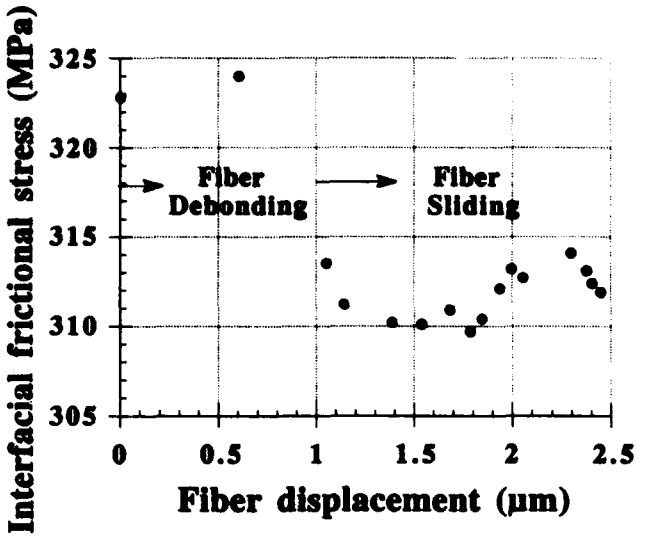

FIG. 5. The relationship between the interfacial frictional stress and the fiber displacement.

coated fiber are clearly seen. Note that the surface roughness appears to be much greater than it actually is as the z-axis is magnified 7× greater than the x-y plane of the fiber surface. Five different areas were chosen for the section analysis by using the Nanoscope III software provided by Digital Corporation (Santa Barbara, CA). The root mean square surface roughness is 18.8 ± 2.2 nm.[1] A SEM micrograph of the pushed-out fiber shows clearly the asperities on the fiber surface (Fig. 7). The size of these asperities is at the same scale as that seen in the AFM image. There is no evidence of wear debris from the β-21S Ti alloy. These observations, along with the information that the interfacial frictional stress (312 MPa) is smaller than the shear yielding strength of the β-21S Ti alloy (525 MPa[13]), lead to the conclusion that the resistance to sliding is primarily due to elastic interactions between the fiber and the matrix.

C. Calculation of friction coefficient

The modeling of the fiber sliding after debonding for fiber pushout tests has been developed by Liang and Hutchinson[9] and modified by Mackin *et al.*[14] who consider an elastic asperities mismatch between the fiber and the matrix. The relationship between the pushout stress and the pushout distance is shown as the following equation:

$$\sigma_u(d) = \frac{E\epsilon_\alpha}{2B}\left\{\exp\left[\frac{2\mu Bt}{R\left(1-\frac{d}{t}\right)}\right]-1\right\} + \left(\frac{2E\mu}{R^2}\right)\exp\left(\frac{-2\mu Bd}{R}\right) \times \int_d^h\left[\exp\left(\frac{2\mu Bz}{R}\right)\right]\delta(z)\,dz \quad (3)$$

with

$$B = \frac{\nu_f E_m}{(1-\nu_f)E_m + (1+\nu_m)E_f} \quad (3a)$$

where ϵ_α is the thermal expansion mismatch, E is the composite modulus, μ is the friction coefficient, $\delta(z)$

FIG. 6. AFM image of the coated fiber.

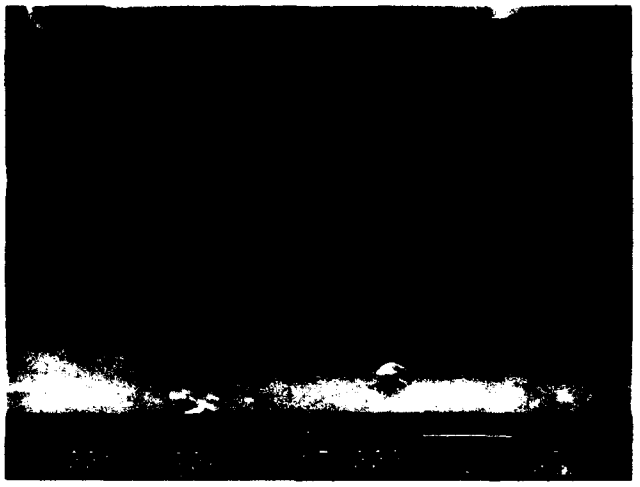

FIG. 7. SEM micrograph of the pushed-out fiber.

is the elastic displacement required for accommodation between fiber and matrix along the embedded length of the fiber axis (z), and h is the thickness of the sample Fig. 8). Here, E and ν denote Young's modulus and Poisson's ratio with subscripts m and f referring to matrix and fiber, respectively.

For the Al_2O_3 fiber reinforced Ti composite bonded at 900 °C

$$\epsilon_\alpha = (\alpha_{Ti} - \alpha_{Al_2O_3})\Delta T = 8.75 \times 10^{-4} \quad (4)$$

$$\Delta T = T_p - T_0 = 900\ ^\circ\text{C} - 25\ ^\circ\text{C} = 875\ ^\circ\text{C} \quad (4a)$$

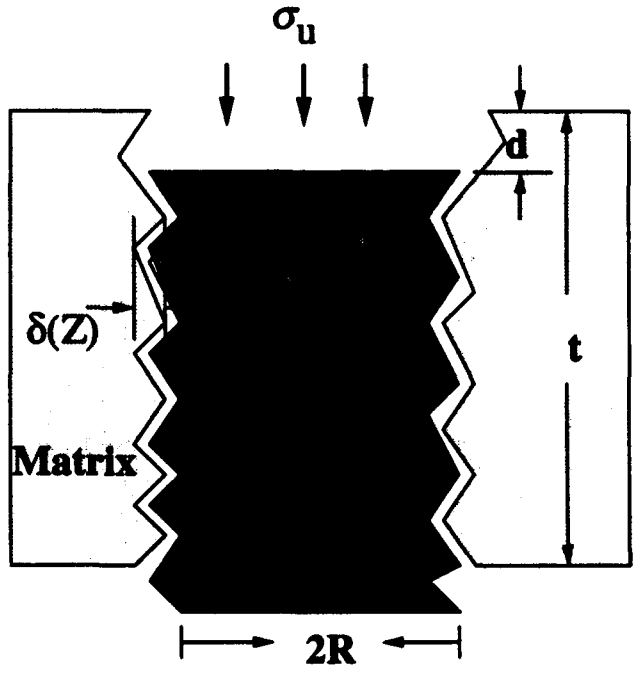

FIG. 8. Schematic diagram of the geometry for the fiber sliding.

where α is the thermal expansion coefficient, T_p is the processing temperature, and T_0 is room temperature.

Moreover, by considering the force balance at the fiber,

$$\tau(d) = \frac{\sigma_u(d)R}{2t}. \quad (5)$$

In this comparison, the asperity mismatch $\delta(z)$, as previously mentioned, is assumed to be an average surface roughness, δ, which is a constant. This surface roughness of the coated Al_2O_3 fiber is 18.8 ± 2.2 nm. Equations (3) and (5) through appropriate substitutions become

$$\tau(d) = \frac{R}{2t}\left\{\frac{E\epsilon_\alpha}{2B}\left[\exp\left(\frac{2\mu Bt}{R\left(1-\frac{d}{t}\right)}\right) - 1\right] + \frac{E\delta}{RB}\left[\exp\left(\frac{2\mu Bt}{R}\right) - 1\right]\right\}. \quad (6)$$

Since all of the variables except friction coefficient μ are known from the experiment, a friction coefficient was determined by matching the theory and the experimental data for the fiber sliding. By considering the variation in the surface roughness of the fiber and the thickness of the specimen, this gives μ a relatively constant value of 0.32 ± 0.02, as shown by the match of theory to experiment in Fig. 9. This value is close to the friction coefficient of 0.26 obtained for a SiC fiber reinforced Ti matrix composite.[14] The evaluation of the frictional stress using the fiber pushout tests and the surface roughness using an AFM provides some insight for the design of high toughness composites. It would appear that modification of the interfacial frictional stress by changing the surface roughness of the fiber is feasible.

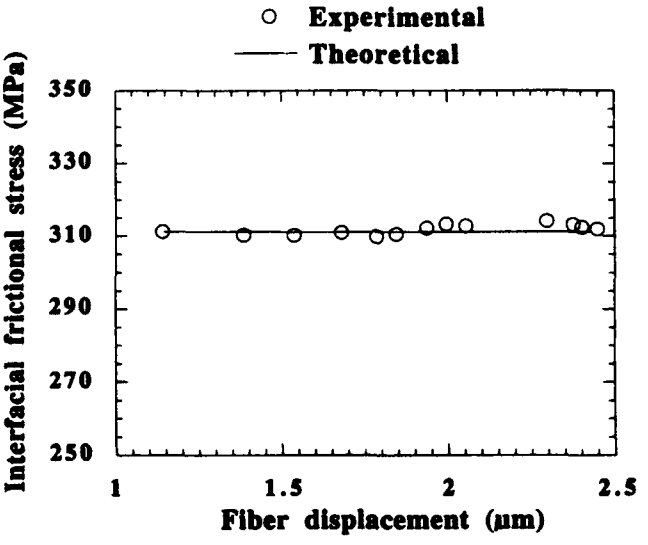

FIG. 9. Comparison between the experimental data and Hutchinson's model.[9]

IV. CONCLUSIONS

Using fiber pushout tests, the mechanical properties of the matrix/fiber interface have been characterized for Al_2O_3 fiber reinforced β-21S Ti alloy. Interfacial fracture was found to occur between the refractory metal and the Y_2O_3 with an interfacial shear strength and interfacial frictional stress of 323 MPa and 312 ± 2 MPa, respectively. Asperity interlocking during fiber sliding contributes to the interfacial frictional stress. By using an atomic force microscope, the surface roughness of the coated Al_2O_3 fiber was found to be 18.8 ± 2.2 nm. Incorporation of the experimental data in Liang and Hutchinson's model[9] gives the friction coefficient to be 0.32 ± 0.02 for the coated Al_2O_3 fiber sliding in a Ti matrix.

ACKNOWLEDGMENTS

This research was supported by 3M/DARPA/ONR Metal Matrix Composite Model Factory Program under subcontract No. GS 01080-KAS and ONR N/N00014-92-J-1962.

REFERENCES

1. Y. M. Yang, S. M. Jeng, and C. J. Yang, Mater. Sci. Eng. **A138**, 155 (1991).
2. J. Wadsworth and F. H. Froes, J. Metals **41**, 12 (1989).
3. J. M. Yang and S. M. Jeng, JOM **44**, 52 (1992).
4. W. W. Gerberich, J. Mech. Phys. Solids **19**, 71 (1971).
5. A. G. Evans, Mater. Sci. Eng. **A143**, 63 (1991).
6. D. B. Marshall, J. Am. Ceram. Soc. **67**, 259 (1984).
7. D. B. Marshall and W. C. Oliver, J. Am. Ceram. Soc. **70**, 542 (1987).
8. W. C. Carter, E. P. Butler, and E. R. Fuller, Scripta Metall. Mater. **25**, 579 (1991).
9. C. Liang and J. W. Hutchinson, Mech. Mater. **14**, 207 (1993).
10. H. F. Wang, W. W. Gerberich, and C. J. Skowronek, Acta Metall. Mater. **41**, 2425 (1993).
11. T. W. Clyne and W. C. Watson, Comp. Sci. Technol. **42**, 25 (1991).
12. D. B. Marshall, Acta Metall. Mater. **40**, 427 (1992).
13. H. E. Dève (unpublished research), 3M Co., St. Paul, MN.
14. T. J. Mackin, P. D. Warren, and A. G. Evans, Acta Metall. Mater. **40**, 1251 (1992).

Part II:

Metal Thickness and Processing Temperature Effects on Ti/Al_2O_3 Interface Fracture

H. F. Wang, S. Venkataraman and W .W. Gerberich
Department of Chemical Engineering and Materials Science, University of Minnesota, Minneapolis, Minnesota 55455

Q. Bai, T. Wu and D. L. Kohlstedt
Department of Geology and Geophysics, University of Minnesota, Minneapolis, Minnesota 55455

ABSTRACT

The interfacial fracture toughness in Ti/Al_2O_3 bimaterial couples has been measured by using four point bending and continuous microscratch tests for several processing temperatures and thicknesses of Ti. The objective was two fold. First, the correlation between the fracture toughness determined from microscratch tests and that obtained from bending tests was investigated. The second objective was to study a small volume effect on interfacial fracture toughness. Fracture surfaces and sample cross sections were analyzed by Scanning Electron Microscopy, Energy Dispersive X-ray Analysis, Auger Electron Spectroscopy and Rutherford Backscattering Spectroscopy. The interfacial fracture toughness measured with four point bending tests increases with increasing applied bonding temperature up to 950°C. Above this temperature the fracture toughness decreases with increasing bonding temperature. This deterioration in toughness is due to an intermetallic phase (Ti_3Al) produced by diffusion at high temperature. For a given thermal treatment, the interfacial fracture toughness decreases with decreasing thickness of Ti. This dependency persisted down to film thicknesses as small as 100 nm. Comparison of the four point bending and microscratch tests suggests that interfacial fracture toughness is critically dependent upon the metal interlayer thickness.

1. INTRODUCTION

Fracture at the metal/ceramic interface is an important issue in the mechanical properties of composites and the decohesion of films and coatings in microelectronics. The mechanism of fracture depends on the stress and fracture toughness of the constituents, the interfacial fracture energy, and the phase angle[1,2]. Therefore, a precise measurement of the interfacial fracture toughness is necessary in order to design suitable interfaces for industrial applications.

Several techniques have been utilized to evaluate the fracture and adhesion strength of metal/ceramic systems such as the peel, bulge and scratch tests[3-5]. Many of these techniques are only qualitative and involve fundamental problems concerning measurable adhesion strength range and data accuracy. In contrast, the four point bending and microscratch adhesion tests are quantitative, and the adhesion strength can be obtained[6-9].

The initial purpose of this work was to develop an accurate standard using two test methods for the systematic measurement of the interfacial fracture toughness. In pursuing this goal with various thickness of films as overlayers or underlayers, a strong thickness effect appeared. The secondary goal then became to quantify this thickness effect and see if it persisted to very small volumes. The study consists of an experimental approach in which the variables such as the test temperature and metal interlayer thickness are changed. Four point bend and microscratch tests were used to measure the interfacial fracture toughness. Surface spectroscopy and fractography were employed to elucidate a few important features with regard to debonding phenomena and interfacial fracture toughness. The relationship between mechanical properties and the chemistry of Ti / Al_2O_3 composite interfaces is also discussed.

2. EXPERIMENTAL PROCEDURES

2.1 Four point bending tests

For measuring the mixed mode interfacial fracture toughness, the four point bending test has been shown to be effective[10]. This was measured with the specimen geometry proposed by Evans[10]. The specimen consists of a bimaterial beam which is evaluated by four point bending as shown in Fig. 1.

To make sandwich specimens for the four point bending tests, Hot Isostatic Press diffusion bonding process (HIP) was performed. As shown in Fig. 1, by sandwiching thin foils of pure Ti (99.8% pure) between two Al_2O_3 plates, the specimens were prepared. Two foils were separated by a gap of 3mm to form a precrack. Applied bonding temperatures of 800°C to 1000°C were chosen. To assess the thickness effect on the interfacial fracture toughness for these Ti/Al_2O_3 composites, different thicknesses of the Ti interlayer which range from 6μm to 127 μm were used. The Al_2O_3 plates and Ti foils were immersed in isopropyl alcohol for 10 min and then cleaned in an ultrasonic cleaner for 20 min. For HIP diffusion bonding, the starting sandwich specimens were wrapped with Ta foils and then encapsulated with glass containers as shown in Fig. 2(a). The glass container was evacuated to 10^{-6} torr and sealed. This was then placed into the hot zone of a high pressure vessel, and HIP bonded in an Ar gas atmosphere as shown in Fig. 2(b). Specimens were first heated to the softening point of the glass under a pressure of 1.75 MPa for 30 min and then pressure and temperature were simultaneously raised to 7 MPa and a fixed temperature which ranged from 800°C to 1000°C. The bonding time was fixed at 1hr.

A notch was cut in the sandwich specimen from the Al_2O_3 side with a low speed diamond saw. Because of the gap between the foils, this forms a well defined precrack. The precracked specimens were placed in a four point bending fixture mounted on a MTS machine. The crosshead speed was 0.06 mm/min with load and displacement being recorded during the test. A critical load drop marks the propagation of a crack along the

interface between Ti and Al_2O_3. This critical load was used to calculate the interfacial fracture toughness. After the four point bending tests were completed, the specimens were cut perpendicular to the bonding interface with a low speed diamond saw. The exposed cross section was then polished. Following this, microstructural observations and chemical analysis of interfaces were conducted with Scanning Electron Microscopy (SEM), Energy Dispersive X-ray Analysis (EDAX), Auger Electron Spectroscopy (AES) and Rutherford Backscattering Spectroscopy (RBS).

2.2 Continuous microscratch tests

2.2.1 Sample processing conditions

A. Sputtering conditions

Titanium Films of 0.1, 0.2, 0.5, 1.0, and 2.0 μm thick were deposited onto single crystal Al_2O_3 substrates by r.f. sputtering. Prior to deposition, the substrates were cleaned with acetone in an ultrasonic cleaner. These were then placed in the sputtering chamber. After evacuating the chamber to a background vacuum $< 5 \times 10^{-7}$ Torr, sputtering was performed at an Ar pressure of 10 mTorr, with a power density of 1.54 W/cm^2. The distance between target and substrate was maintained at 75mm during the deposition. The deposition rate was about 100Å/min and the substrate temperature during deposition was not more than 80 °C.

B. Electron beam evaporation conditions

Electron beam evaporation was used to prepare the Ti films which were used to characterize the temperature effect. Before the evaporation process, the chamber was evacuated to 10^{-6} torr. A deposition rate of 20 Å/s and power 1.5 kW was then used to produce 0.8 μm thick Ti films.

C. Heat treatment conditions

To minimize the loss of Ti during the heat treatment, samples were housed in Ti capsules. The sample temperature was controlled to ± 1°C and was monitored by Pt/Pt13%Rh thermocouples located within 15 mm of the samples. Using various gases or gas mixtures such as H_2, Ar, CO/CO_2 and CO/Ar, the oxygen partial pressure around the samples was controlled and varied in the range of 10^{-22} - 10^{-4} atm. The values of oxygen partial pressure were measured by a

zirconia oxygen partial pressure sensor located next to the sample capsule. The heating and the cooling rates were generally ~20 °C/min.

2.2.2 Microscratch tests

Microscratch tests were performed by driving a conical diamond indenter both in the vertical and horizontal directions at the same time. Before the test, the indenter was located just above the surface of the sample allowing the test to be started at zero applied load. The total scratch distance and scratch speed were set at 120 μm and 0.5 μm/s, respectively. The speed of the vertical movement of the indenter was 15 nm/s. When the film delaminated from the substrate, an abrupt drop in the load occurred. This critical load is used to calculate the interfacial fracture toughness.

In general, twenty microscratch tests were performed on each sample. After the microscratch tests, the resulting scratch tracks and delaminated areas were examined with a scanning electron microscope and an optical microscope with Nomarski contrast to determine the width of the track (2a), the area of the thin film that debonds from the substrate (A_d), the length of the debonded region (B) and the angle (θ) enclosed by the fan-shaped debonded area. The critical load (P_{cr}) is determined from the microscratch data. These values were used to calculate the interfacial fracture toughness. Values for the interfacial fracture toughness and the interfacial fracture energy for scratch tests were calculated followed by chemical analysis of the Ti/Al_2O_3 specimens using RBS.

3. RESULTS

3.1 Determination of interfacial fracture toughness

3.1.1 Four point bending tests

The critical load (P) measured from the load-displacement curve is used to calculate the interfacial fracture toughness (K_c) (or interfacial fracture energy (G_c)) as follows[9,10]: (The details are given in the appendix.)

$$M = \frac{PL}{2b}$$

$$G_c = \frac{(1-\nu_2^2)M^2}{2E_2}\left(\frac{1}{I_2} - \frac{\lambda}{I_c}\right)$$

$$\lambda = \frac{E_2(1-\nu_1^2)}{E_1(1-\nu_2^2)}$$

$$|K_c| = \{4\cosh^2(\pi\varepsilon)\, G_c / [(1-\nu_1)/\mu_1 + (1-\nu_2)/\mu_2]\}^{1/2}$$

$$\varepsilon = (1/2\pi)\ln\{[(3-4\nu_1)/\mu_1 + 1/\mu_2][(3-4\nu_2)/\mu_2 + 1/\mu_1]^{-1}\}$$

where E, μ and ν are Young's modulus, the shear modulus and Poisson's ratio, respectively. The subscripts 1, 2 and c refer to materials 1 and 2 and the overall composite (Fig. 1). Here, ε is the bimaterial constant , I is the second moment of inertia and L and b are depicted in Fig. 1.

3.1.2. Continuous microscratch tests

The average shear stress (τ) and normal stress ··) in the delaminated region are the function of a, A_d, B, θ and L_{cr}. The critical strain energy, G_c, (or interfacial fracture energy) released through the thickness of the film can be expressed as[7]

$$G_c = \sum\left(\frac{\tau_{ij}^2}{2\mu}t + \frac{\sigma_{ij}^2}{2E}t\right) \qquad (1)$$

where t is the thickness of the film , μ and E are the shear modulus and Young's modulus of the film respectively. For more details see reference 7. Therefore, the interfacial fracture toughness, K_c, can be calculated using the fracture mechanics result[11],

$$K_c = \sqrt{\frac{2\mu G_c}{1-\nu}} \qquad (2)$$

3.2 Effect of Ti thickness

3.2.1. Four point bend tests

The interfacial fracture toughness was measured for four different thicknesses of the Ti interlayer at a fixed bonding temperature of 900°C. The interfacial fracture toughness (or interfacial fracture energy) increases from 1.42 MPa-$m^{1/2}$ to 3.45 MPa-

$m^{1/2}$ (or 9.6 J/m^2 to 45.1 J/m^2) as the thickness of the Ti interlayer was increased from 6 μm to 127 μm, as shown in Fig. 3.

3.2.2. Continuous microscratch tests

In each scratch experiment, the load increases as the the indentor goes into and across the film, building a stress ahead of it. At a critical load, the film delaminates. The SEM observations in Fig. 4 illustrate the features that are representative of typical scratch tracks. This critical load drop which corresponds to the film delamination from the substrate along with the area of delamination were used to evaluate the i cial fracture toughness (or interfacial fracture energy) of the samples. The interfacial fracture toughness increases from 0.2 MPa-$m^{1/2}$ to 1.46 MPa-$m^{1/2}$ as the Ti film thickness increases from 0.1 μm to 2 μm (Fig. 5). The interfacial fracture energy correspondingly increases from 0.28 J/m^2 to 14.7 J/m^2.

3.3 Effect of temperature

3.3.1. Four point bend tests

The interfacial fracture toughness was measured at different applied bonding temperatures for a 25 μm thickness Ti interlayer. The relationship between interfacial fracture toughness (or interfacial fracture energy) and bonding temperature is shown in Fig.6. The interfacial fracture toughness (or interfacial fracture energy) increases from 2.3 MPa-$m^{1/2}$ to 2.66 MPa-$m^{1/2}$ (or 25.4 J/m^2 to 34.1 J/m^2) as the bonding temperature increases from 800°C to 950°C. Then the interfacial fracture toughness drops to 1.9 MPa-$m^{1/2}$ (or 16.9 J/m^2) when the bonding temperature is further raised to 1000°C. The SEM cross-sectional view of a specimen which was bonded at 1000°C is shown in Fig.7(a). A reaction layer exists between Ti and Al_2O_3. A slight contrast difference exists between the reaction layer and the Ti in the backscattering electron image in Fig. 7(b). From the X-ray map in Fig. 8, the diffusion of Al into Ti is seen to be much greater than that of Ti into Al_2O_3. The morphology of the fracture surfaces of the specimens which

were bonded at 1000°C and tested with four point bending are shown as Fig. 9. The presence of a continuous reaction layer is on both sides of the Ti indicates that the crack propagates in the reaction layer between the Ti and Al_2O_3. The composition of the reaction product at the interface is analyzed by using EDAX with the semi-quantitative data being shown in Fig. 10. From the measured atomic % of Ti and Al, the reaction layer between Ti and Al_2O_3 is identified as Ti_3Al. Because the Ti_3Al intermetallic alloy is very brittle[12,13], it will reduce the fracture toughness of the interface. It is expected that when the bonding temperature is 1000°C, a great deal of Ti_3Al is produced which will decrease the interfacial fracture toughness of Ti / Al_2O_3 composites. This is consistent with Tressler and Moore's[14,15] results on the deterioration of Ti/Al_2O_3 composite strength caused by the presence of Ti_3Al produced during processing.

The fracture surface of the Ti interlayer where the crack crossed from the upper to the lower interface also has a brittle appearance. There are two possibilities for this behavior. The first one is because the metal interlayer is sandwiched between the Al_2O_3, causing constrained plastic deformation with the stress reaching a much higher value than that in the unconstrained elastic/plastic solid[16,17]. The second possibility is that as oxygen diffuses into the Ti during the HIPing process, the Ti interlayer embrittles. Chemical analysis of the Ti interlayer after the HIPing shows that the oxygen concentration is about 15 at% (Fig. 11).

3.3.2. Continuous microscratch tests

Twenty samples were heat treated at temperatures of 400°C - 1000°C in an oxygen partial pressure of 10^{-22} atm for 3 hrs. For samples annealed at temperatures below 600°C, the oxygen partial pressure cannot be measured by the oxygen sensor. One sample was annealed at 400°C for 20 hrs.

The four samples annealed at 400°C and 450°C for 4 hrs as well as the sample annealed at 400°C for 20 hrs, showed very strong adhesion of the Ti film to the Al_2O_3 substrate, such that no

failure could be produced by microscratch tests using a diamond indenter with tips of radius 1, 5 and 10 μm. SEM observations showed no sign of film delamination from the substrate.

Four samples were heat treated at 500°C and 550°C for 3 hrs. For these samples, delamination of the films from the substrates was induced. The interfacial fracture toughness (or interfacial fracture energy) for the samples annealed at 500°C and 550°C is 0.53 MPa-$m^{1/2}$ and 0.43 MPa-$m^{1/2}$ (or 2.4 J/m^2 and 1.6 J/m^2), respectively, as shown in Fig. 12. At higher temperatures, 1000°C, the interfacial fracture toughness decreased substantially. For samples treated at 1000°C, the interfacial fracture toughness (or the interfacial fracture energy) is 0.18 MPa-$m^{1/2}$ (or 0.3 J/m^2).

RBS spectra were obtained from the specimens as exemplified by Fig.13. In an RBS spectrum, the normalized yield (*i.e.*, the number of α-particles scattered into the detector normalized to the total incident beam dosage, the detector solid angle and the channel width of the multichannel analyzer) is plotted against the energy of the backscattered α-particles. The element markers on the energy axis indicate where the yield edge for a particular element should be if that element were present at the surface of the specimen. Thus, from Fig. 13(a), for instance, it is clear that Ti is present at the surface whereas Al is not. Composition profiles can be obtained by simulating the RBS spectrum of a hypothetical sample. The parameters of the hypothetical sample are adjusted until its simulated RBS spectrum is deemed sufficiently close to the spectrum of the real sample. The composition profiles in the hypothetical specimen are then considered to be a good approximation of those in the real sample.

Heat treatment produced marked effects on the compositional structure of the samples. As shown in Fig. 13(a), in an "untreated" specimen, a film of almost pure Ti (the thickness of this film is about 750 nm from the RBS simulation) overlies a layer of Al and O, presumably forming Al_2O_3. A small amount of O is present at the surface, but the concentration of O decreases to zero going into the Ti film. For a specimen heat treated for 3 hrs at 500°C, the spectrum (Fig. 13(b)) is similar to that for the untreated specimen except that the oxygen signal remains non-zero from the surface marker to the lower energies, and that the Ti yield is lower. This result demonstrates

that although the basic structure of the specimen has not changed, there is a significant amount of oxygen present throughout the Ti film. For the sample treated at 900°C for 3 hrs, the RBS spectrum has fundamentally changed (Fig. 13(c)). The energy edge for Al appears at a higher energy than for the other two samples, accompanied by a yield step in the lower-energy portion of the Ti peak. These observations indicate that a layer of a Ti-Al compound exists between the Ti film and the Al_2O_3 substrate. In addition, the oxygen content in the Ti film is also higher. These results are consistent with chemical analyses obtained by SEM, EDAX and AES.

4. DISCUSSION

As shown in Fig. 3, the interfacial fracture toughness increases with increasing thickness of metal. A larger plastic energy dissipation within the Ti interlayer contributes in the form of near tip deformation and crack blunting during the interfacial crack propagation as the Ti layer becomes thicker. A similar thickness effect of metal interlayer on the interfacial fracture toughness has also been found in the Au/Al_2O_3[16,17] and Cu/glass systems[18-21].

The interfacial fracture energy measured from continuous microscratch and four point bending tests ranges from 0.28 J/m^2 to 14.7 J/m^2 and 9.6 J/m^2 to 45.1 J/m^2 respectively. These values are larger or within the range of typical work of adhesion in metal/ceramic systems[22] (0.05 J/m^2 - 1.0 J/m^2). Since the interfacial fracture energy is equal to the work of adhesion and the nonlinear energy dissipation in the metal[23], it is seen that the work of adhesion is only a small portion of the interfacial fracture energy. The fraction of the irreversibly dissipated plastic energy is higher than 80% for the thick Ti. Correlation between the four point bending and microscratch tests for different thickness of Ti was made as shown in Fig. 14. It is seen that the interfacial fracture toughness measured by these two techniques are in reasonable agreement. The interfacial fracture toughness obtained from microscratch tests is a little larger than the value determined from the four point bending tests in the region of 1-10 μm. This might be expected possibly because the mixed mode fracture process in these two tests is not the same. In the four point bending tests, the phase angle of loading Ψ is about 45° where $\Psi = \tan^{-1}(K_{II} / K_I)$. This means there is an equal

amount of K_I and K_{II} in this fracture condition. Here, K_I and K_{II} are mode I (opening mode) and mode II (in-plane shear mode) stress intensity factors respectively. In contrast, the increasing shear stress ahead of the sliding indentor tip during the continuous microscratch tests causes the delamination of the films from the substrates. It is apparent that the relative shear stress component in microscratch tests is higher than that in the four point bending tests. Therefore, the phase angle of loading is larger in microscratch tests, resulting in an increase in interfacial fracture toughness[6] due to roughness-induced shielding and plastic dissipation during the fracture process[24-25].

A comparison of the fracture energy obtained from the four point bending tests and the continuous microscratch tests for different processing temperatures shows consistent results. The interfacial fracture toughness measured from the microscratch tests is an order magnitude smaller than the value obtained from four point bending tests. The most likely cause of this behavior is the thickness variable since, as given in equation (1), the interfacial fracture energy should increase proportional to the thickness. The Ti layer thickness which differed by a factor of 30 and the difference in phase angle as discussed above account for most of the remaining difference in interfacial fracture energy observed. Additionally, the residual stress developed in the Ti film during the annealing process for the microscratch tests may be another factor to cause some variation.

These results show that a reasonably quantitative evaluation of the adhesion strength in metal/ceramic interfaces is possible. The applied bonding temperatures and thicknesses of metal interlayers have a great effect on the interfacial fracture toughness (or interfacial fracture energy) of the composites. Therefore, by changing these processing conditions, either "weak" or "strong" interfaces can be obtained[26]. It has been shown that the thermomechanical properties of the interfaces have a dominant effect on the macroscopic mechanical properties of composites and thin films[26]. For example, systematic studies of the trends in the fracture energy for a variety of interfaces could be very useful to the design of composites and thin films.

5. SUMMARY AND CONCLUSIONS

Four point bending and microscratch tests were performed successfully to measure interfacial fracture toughness in Ti/Al_2O_3 composites. Interfacial fracture toughnesses determined from four point bending and continuous microscratch tests are in reasonable agreement and show an increasing trend with increasing film thickness. This is due to the plastic energy dissipation of the Ti during the fracture process. The interfacial fracture toughness (or interfacial fracture energy) reaches a maximum value of 2.66 MPa-$m^{1/2}$ (or 34.1 J/m^2) with a bonding temperature of 950°C. The presence of the intermetallic compound Ti_3Al produced during bonding at 1000°C deteriorates the fracture toughness of the Ti/Al_2O_3 composite. The interfacial fracture toughness measured from continuous microscratch tests of thin films ranges from 0.18 to 1.46 MPa-$m^{1/2}$ (or 0.3 to 14.7 J/m^2) depending on annealing temperature and thickness of Ti.

ACKNOWLEDGMENTS

This research was supported by 3M/DARPA/ONR Metal Matrix Composite Model Factory Program under subcontract No. GS 01080 - KAS and ONR N/N00014-92-J-1962 (H.F. Wang and Q. Bai) and Center for Interfacial Engineering at the University of Minnesota under grant No. NSF/CDR-8721551(S. Venkataraman and T. Wu). The authors wish to acknowledge Mr. C.J. Skowronek and Phil Bebruzzi of the Metal Matrix Composites division, 3M Company and Chien-Li Lin in the Department of Chemical Engineering and Materials Science, University of Minnesota for sample preparation. Dr. J. C. Nelson was also involved in helpful discussion. Their assistance is gratefully acknowledged.

REFERENCES

1. M.D. Thouless and A.G. Evans, ***Scrip. Metal. et. Mater.***, 24, 1507 (1990).

2. H.M. Jensen, ***Acta. Metall. Mater.*** **38**, 2637 (1990).

3. K.S. Kim and N. Aravas, ***Int. J. Solids Struc.***, **24**, 417 (1988).

4. A.J. Perry, ***Thin Solid Films***, **107**, 167 (1983).

5. P.A. Steinmann, Y. Tardy and H.E. Hintermann, ***Thin Solid Films*, 154**, 333 (1987).

6. A.G. Evans, M. Ruhle , B.J. Dalgleish and P.G. Charalambides, ***Mater. Sci. Eng.* A126**, 53 (1990).

7. S.Venkataraman, D.L. Kohlstedt and W.W. Gerberich, ***J. Mater. Res.*, 7**, 1126 (1992).

8. P.G. Charalambides, J. Lund, A.G. Evans and R.M. McMeeking, ***J. Appl. Mech.*, 56**, 77 (1989).

9. H.C. Cao and A.G. Evans, ***Mech. Mater.*, 7**, 295 (1989).

10. P.G. Charalambides, H.C. Cao, J. Lund and A.G. Evans, ***Mech. Mater.*, 8**, 269 (1990).

11. G.E. Dieter, ***Mechanical Metallurgy*** (McGraw-Hill Publications, New York, 1988), P. 353.

12. H.A. Lipsitt, D. Shechtman and R.E. Schafrik, ***Metall. Trans.*, 11A**, 1370 (1980).

13. H.T. Kestner, C.H. Ward, T.F. Broderick and M.J. Kaufman, ***Scripta Met.*, 23**, 1697 (1989).

14. R.E. Tressler and T.L. Moore, ***Met. Eng. Quarterly*, 2**, 16 (1971).

15. R.E. Tressler, T.L. Moore and R.L. Crane, ***J. Mater. Sci.*, 8**, 151 (1973).

16. I.E. Reimanis, B.J. Dalgleish, M. Brandy, M. Ruhle and A.G.Evans, ***Acta. Metall. Mater.*, 38**, 2645 (1990).

17. I.E. Reimanis, B.J. Dalgleish and A.G.Evans, ***Acta. Metall. Mater.*, 39**, 3133 (1990).

18. R.M. Cannon, V. Jayaram, B.J. Dalgleish and R.M. Fisher, ***Ceramic Microstructure '86***, edited by J.A. Pask and A.G. Evans (Plenum Press, New York, 1987). P. 959.

19. R.M. Cannon, R.M. Fisher and A.G. Evans, ***Mat. Res. Soc. Symp. Proc.*,**

54, 799 (1986).

20. T. Suga and G. Elssner, ***Mat. Res. Soc. Symp. Proc.*,40**, 203 (1985).

21. A.G. Evans and J.W. Hutchinson, ***Int. J. Solids Struc.*, 20**, 455 (1984).

22. J.T. Klomp, ***Fundamental of Diffusion Bonding***, edited by Yoichi Ishida (Elsevier Amsterdam, 1987), P. 3.

23. A.G. Evans and M. Ruhle, ***Mater. Res. Soc. Bull.*, 10**, 46 (1990).

24. A.G. Evans and J.W. Hutchinson, ***Acta. Metall.*, 37**, 909 (1989).

25. T.S.Oh, J. Rodle, R.M. Cannon and R.O. Ritchie, ***Acta. Metall.*, 36**, 2083 (1988).

26. A.G.Evans, ***Mater. Sci. Eng.* A143**, 63 (1991).

27. M.F. Kanninen and C. H. Popelar, ***Advanced Fracture Mechanics*** (Oxford University Press, New York , 1985).

APPENDIX

The strain energy release rate (G_C) can be calculated from consideration of the energies in the uncracked section, and in a section of the lower beam beneath the crack (Fig.1). From Euler- Bernoulli beam theory and the plane strain condition, these energies can be expressed in terms of the applied moment (M)

$$U = \frac{(1 - \nu^2)M^2}{2EI} \qquad \text{(A1)}$$

where U is the strain energy per unit cross section, I is the second moment of inertia per unit width and ν is the Poisson's ratio.

$$G_c = \frac{M^2}{2E_2}(1-\nu_2^2)(\frac{1}{I_2} - \frac{\lambda}{I_c})$$

$$\lambda = \frac{E_2(1-\nu_1^2)}{E_1(1-\nu_2^2)} \qquad \text{(A2)}$$

E is Young's modulus and I_c the moment of inertia of a bimaterial beam which is equal to

$$I_c = \frac{h_1^3}{12} + \lambda\frac{h_2^3}{12} + \lambda\, h_1 h_2 \frac{(h_1+h_2)^2}{4(h_1+\lambda\, h_2)} \qquad \text{(A3)}$$

$$I_2 = \frac{h_2^3}{12}$$

where h_1 and h_2 are the thicknesses of upper beam and lower beam respectively (Fig. 1).

The stress intensity factor (or interfacial fracture toughness) K_c can also be related to the plane strain energy release rate (or interfacial fracture energy) G_c by[27]

$$G_c = [(1-\nu_1)/\mu_1 + (1-\nu_2)/\mu_2]K_c\overline{K_c}/4\cosh^2(\pi\varepsilon) \qquad \text{(A4)}$$

Furthermore, since

$K_c\overline{K_c} = |K_c|^2$

$$|K_c| = \{4\cosh^2(\pi\varepsilon)\, G_c / [(1-\nu_1)/\mu_1 + (1-\nu_2)/\mu_2]\}^{1/2} \qquad \text{(A5)}$$

All dimensions are shown in Fig 1. The moment per unit width M is given by $M = \frac{PL}{2b}$, with P being the critical load determined from load- displacement curve, L the spacing between the inner load and outer load points, and b the width of the specimen. The critical interfacial strain energy release rate, here defined as interfacial fracture energy, can be obtained from equation (A2). Therefore, the interfacial fracture toughness can be calculated from equation (A5).

LIST OF FIGURES

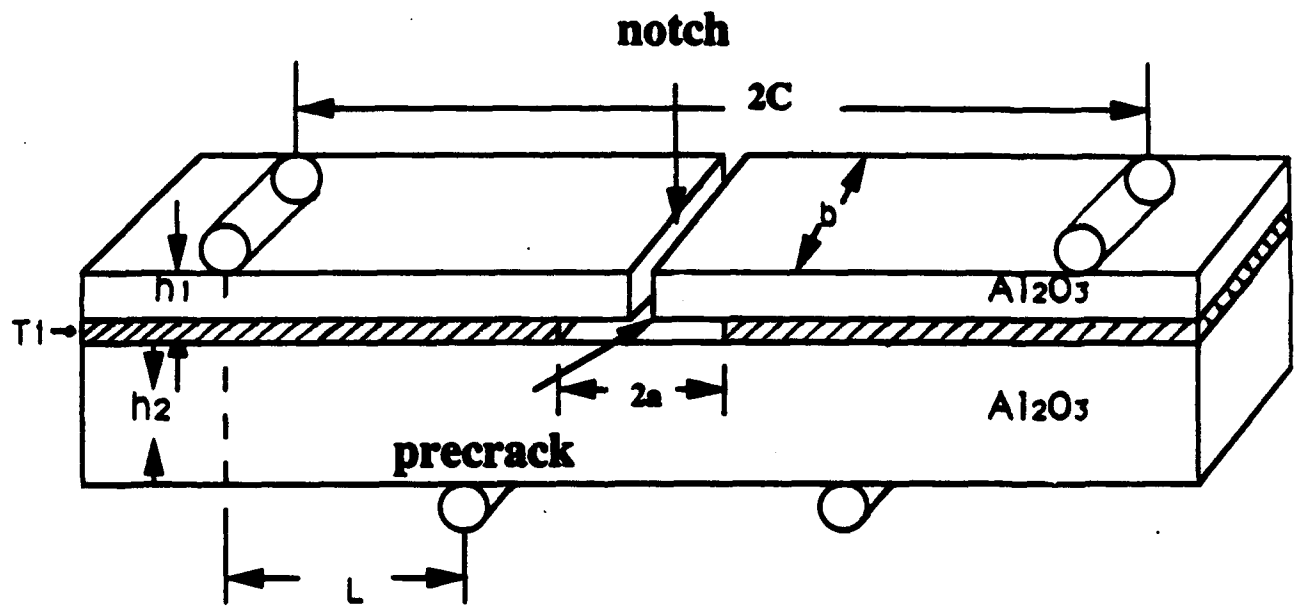
notch
2C
b
h1
Al2O3
T1
h2
2a
Al2O3
precrack
L

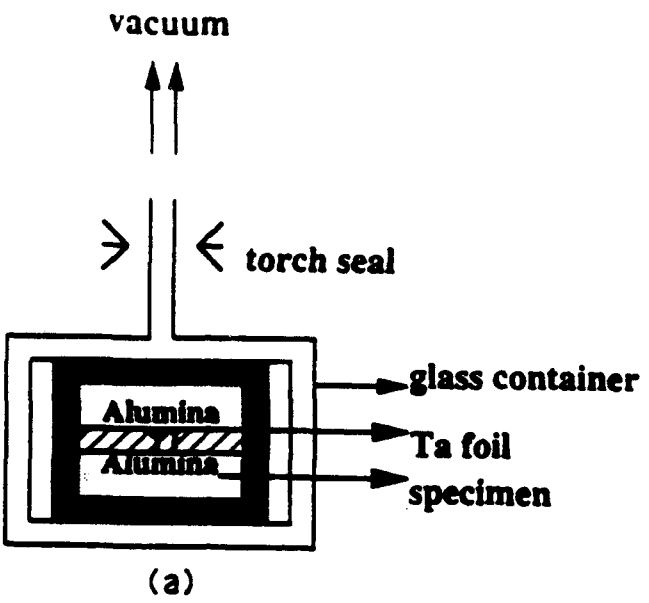
vacuum
torch seal
glass container
Alumina
Ta foil
Alumina
specimen

(a)

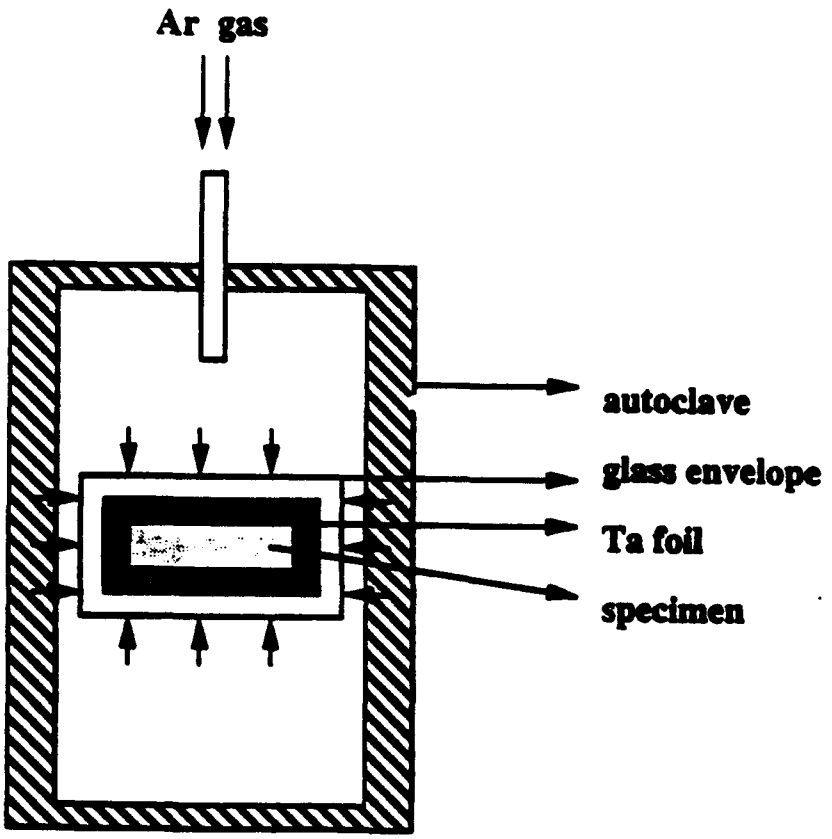
Ar gas
autoclave
glass envelope
Ta foil
specimen

(b)

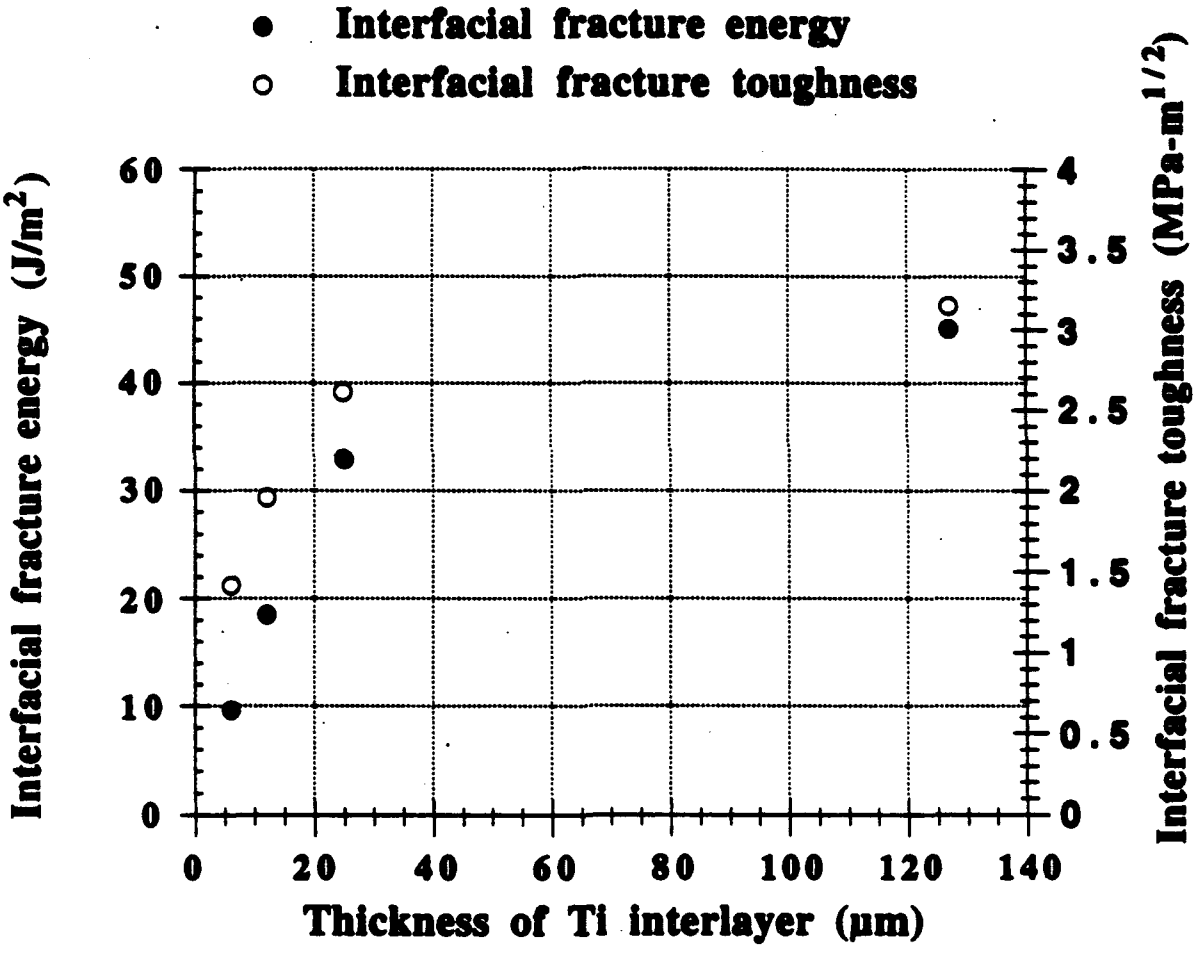
● Interfacial fracture energy
○ Interfacial fracture toughness
Interfacial fracture energy (J/m²)
Interfacial fracture toughness (MPa-m^1/2)
Thickness of Ti interlayer (μm)
0
10
20
30
40
50
60
0
0.5
1
1.5
2
2.5
3
3.5
4
0
20
40
60
80
100
120
140

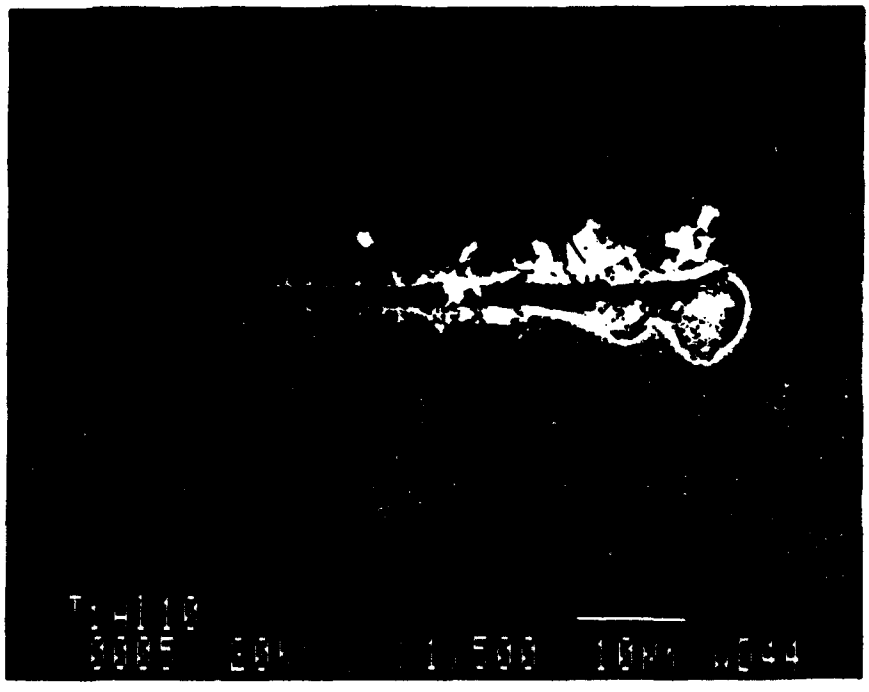

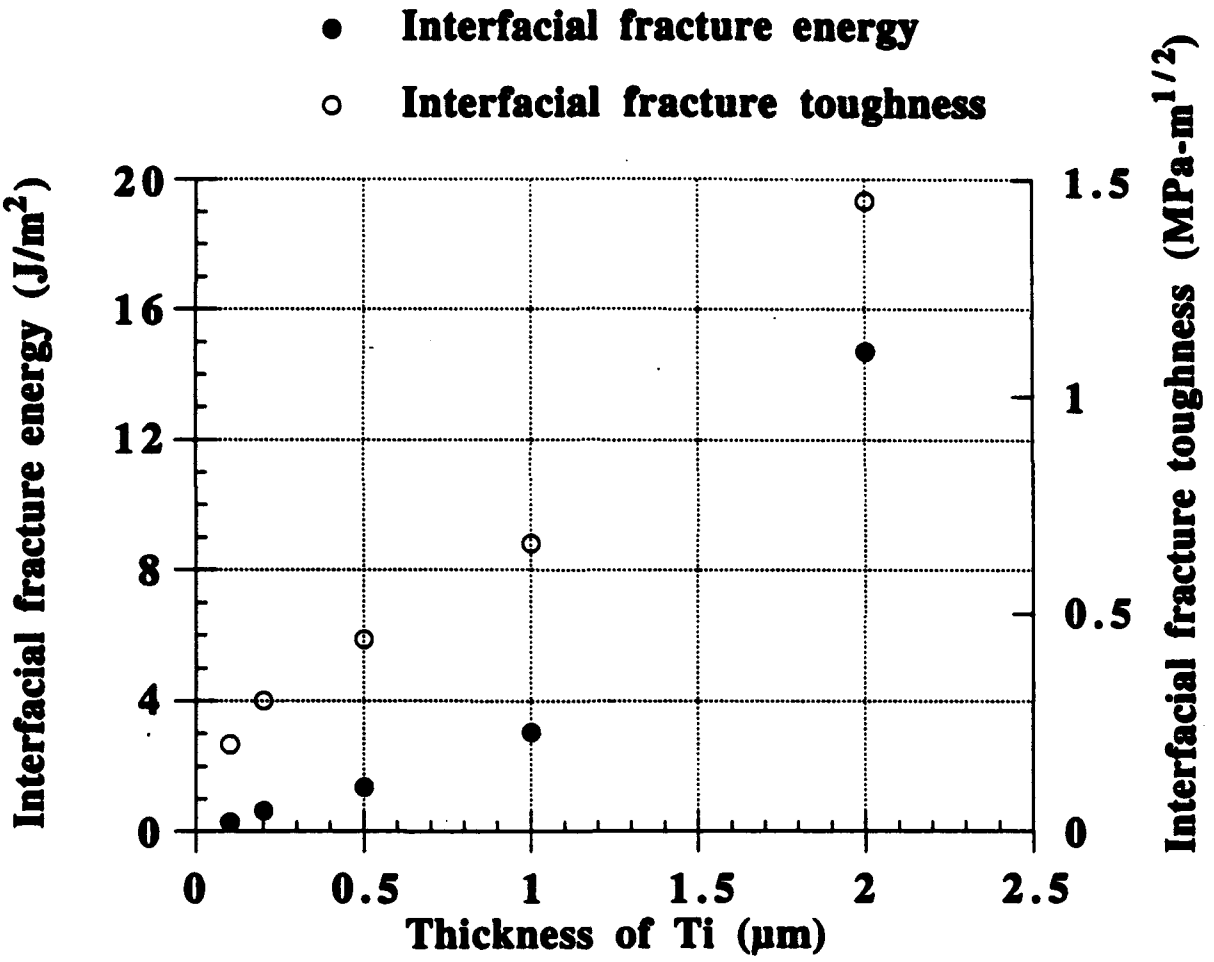
Interfacial fracture energy
Interfacial fracture toughness
Interfacial fracture energy (J/m^2)
Interfacial fracture toughness (MPa-m$^{1/2}$)
20
16
12
8
4
0
1.5
1
0.5
0
0
0.5
1
1.5
2
2.5
Thickness of Ti (μm)

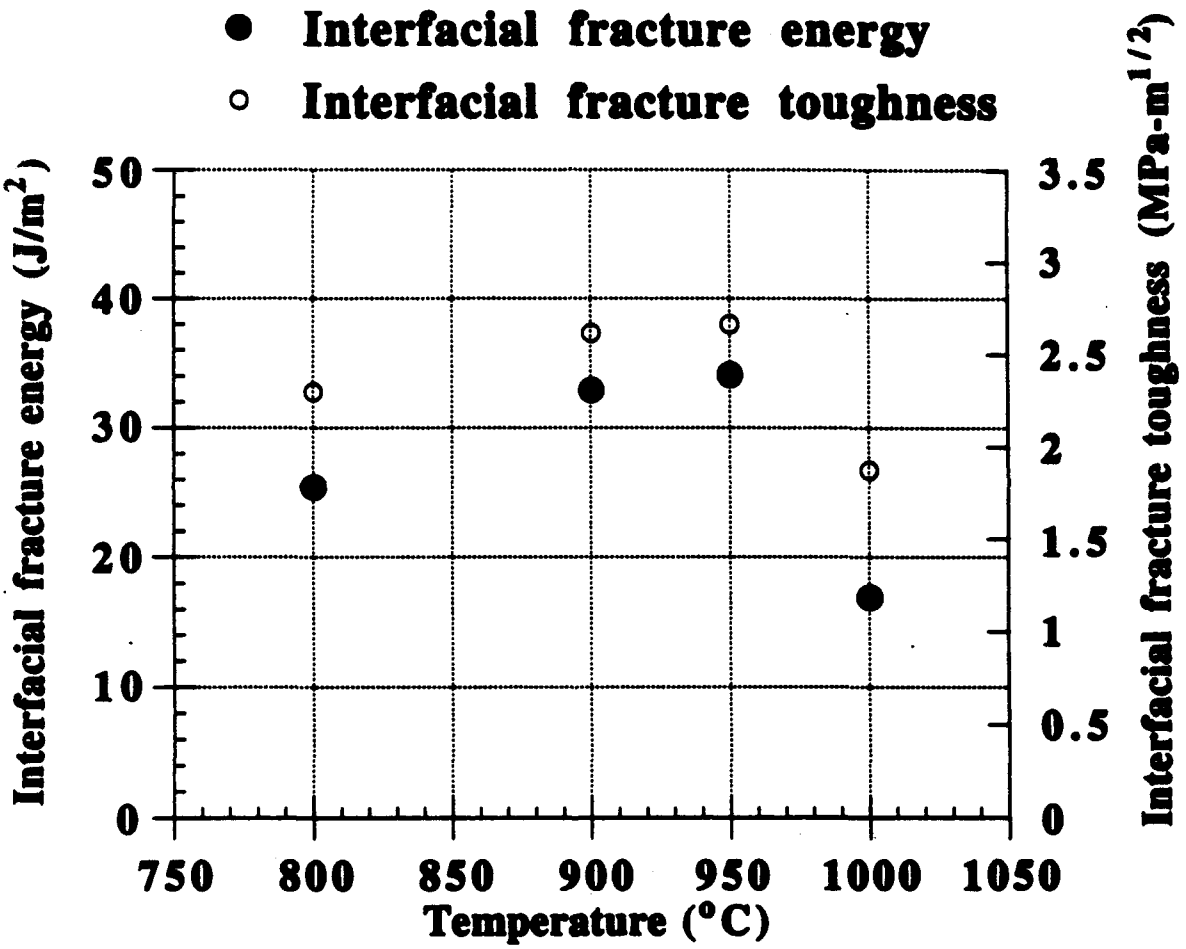
Interfacial fracture energy
Interfacial fracture toughness
Interfacial fracture energy (J/m^2)
Interfacial fracture toughness (MPa-m$^{1/2}$)
0
10
20
30
40
50
0
0.5
1
1.5
2
2.5
3
3.5
750
800
850
900
950
1000
1050
Temperature (°C)

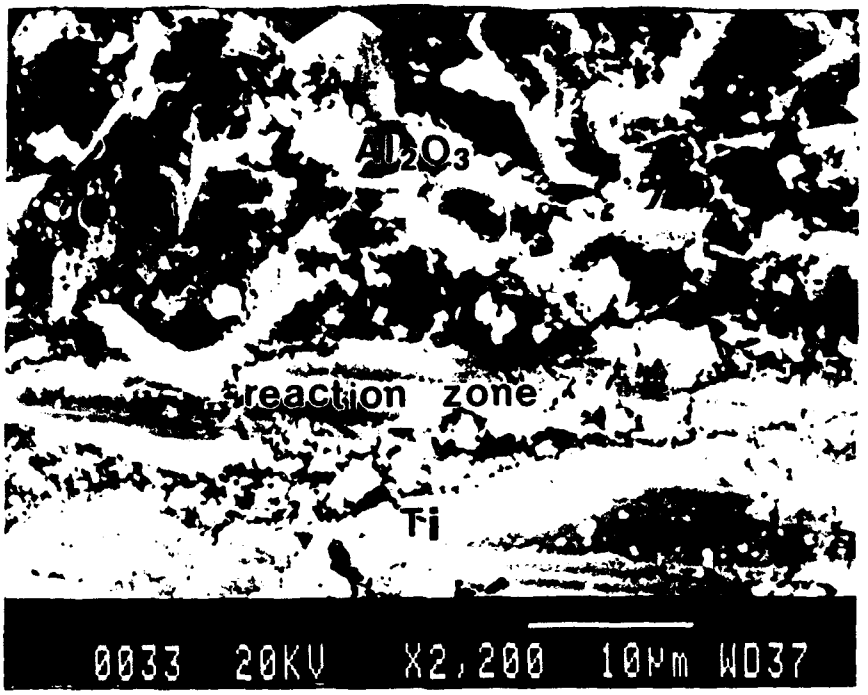
Al_2O_3
reaction zone
Ti
0033 20KV X2,200 10µm WD37

(a)

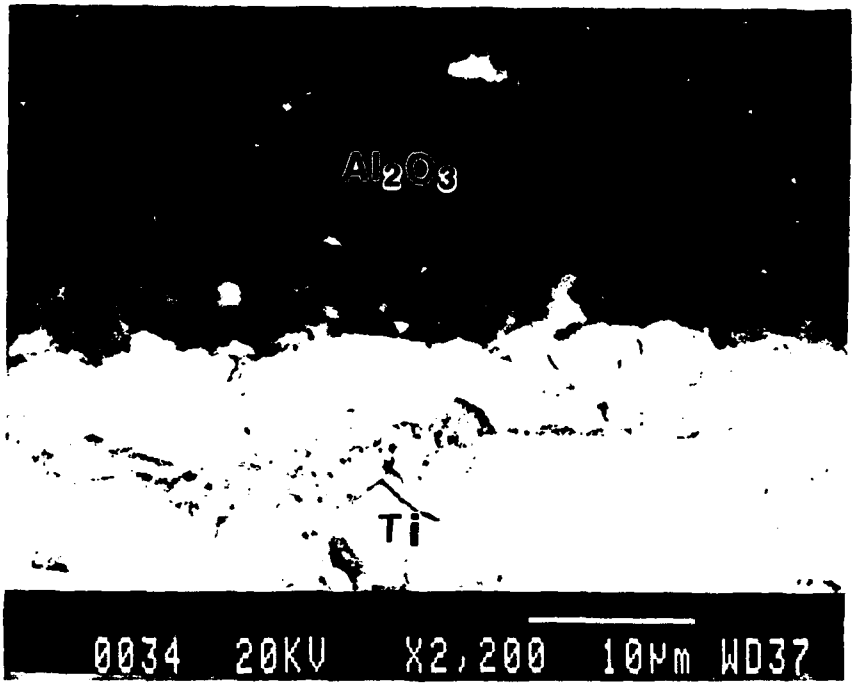
Al_2O_3
Ti
0034 20KV X2,200 10µm WD37

(b)

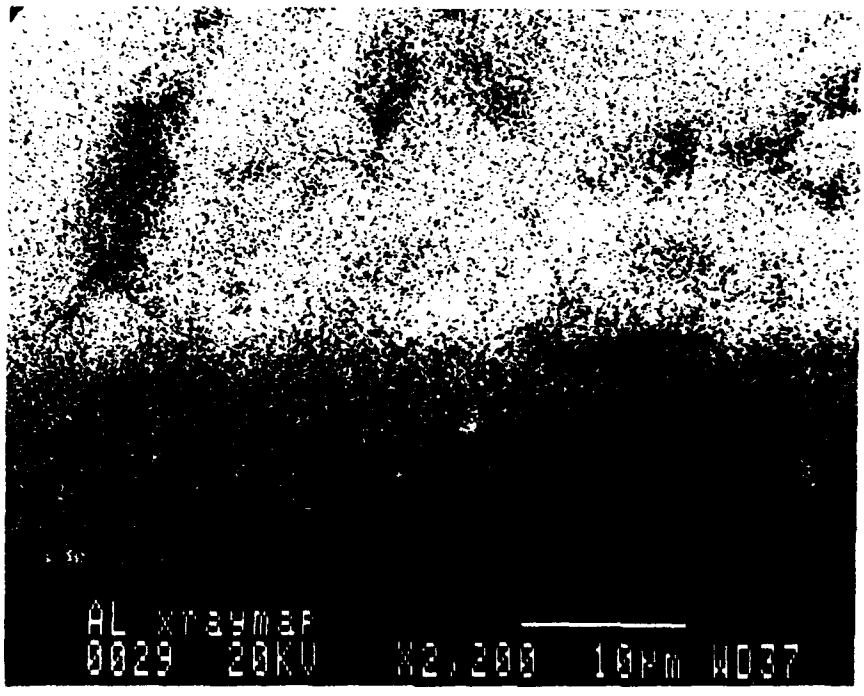
AL xraymap
0029 20KV X2,200 10Pm WD37

(a)

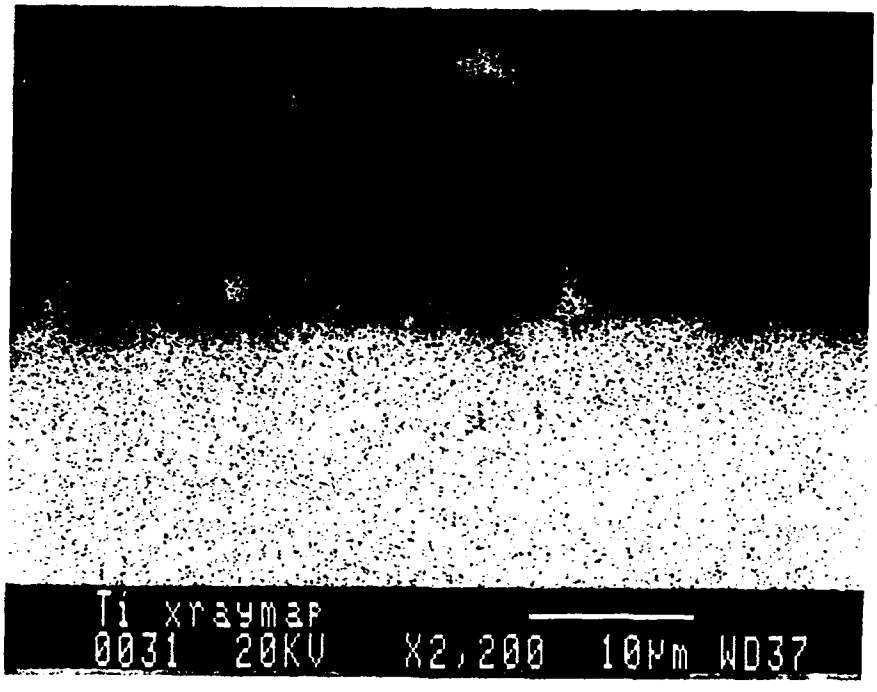
Ti xraymap
0031 20KV X2,200 10Pm WD37

(b)

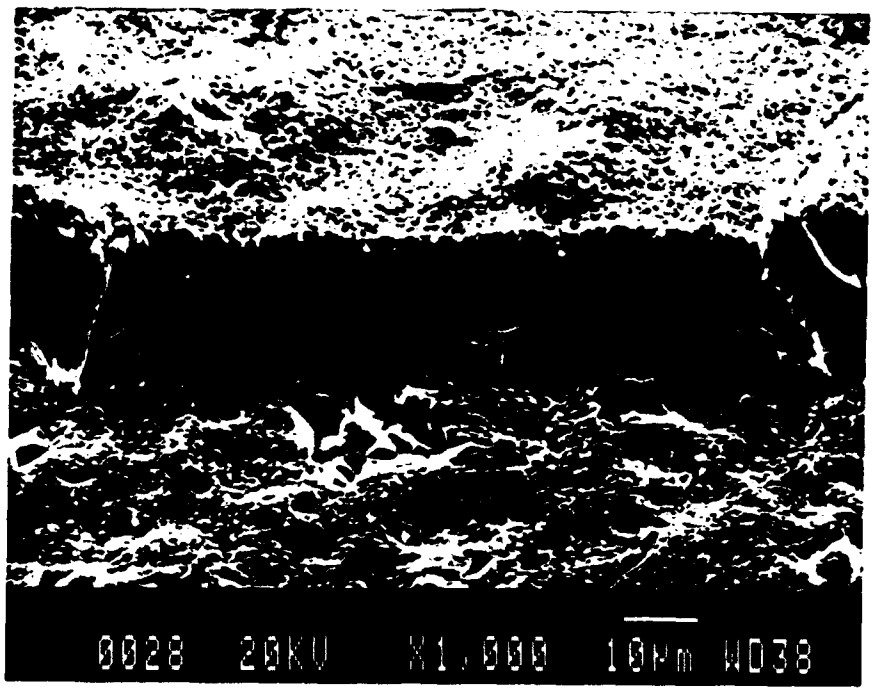
0028 20KV X1,000 10Pm WD38

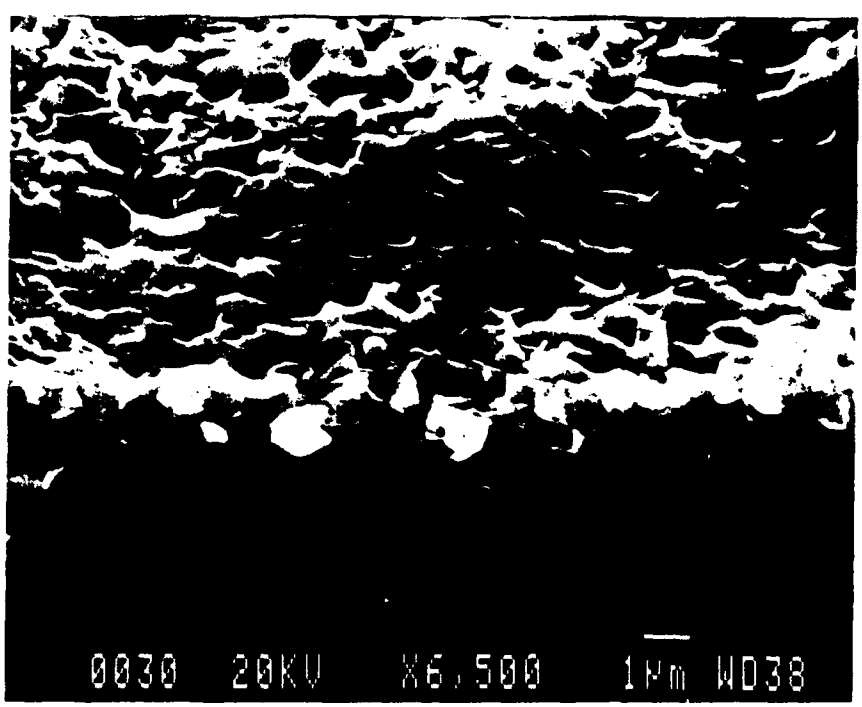
0030 20KV X6,500 1Pm WD38

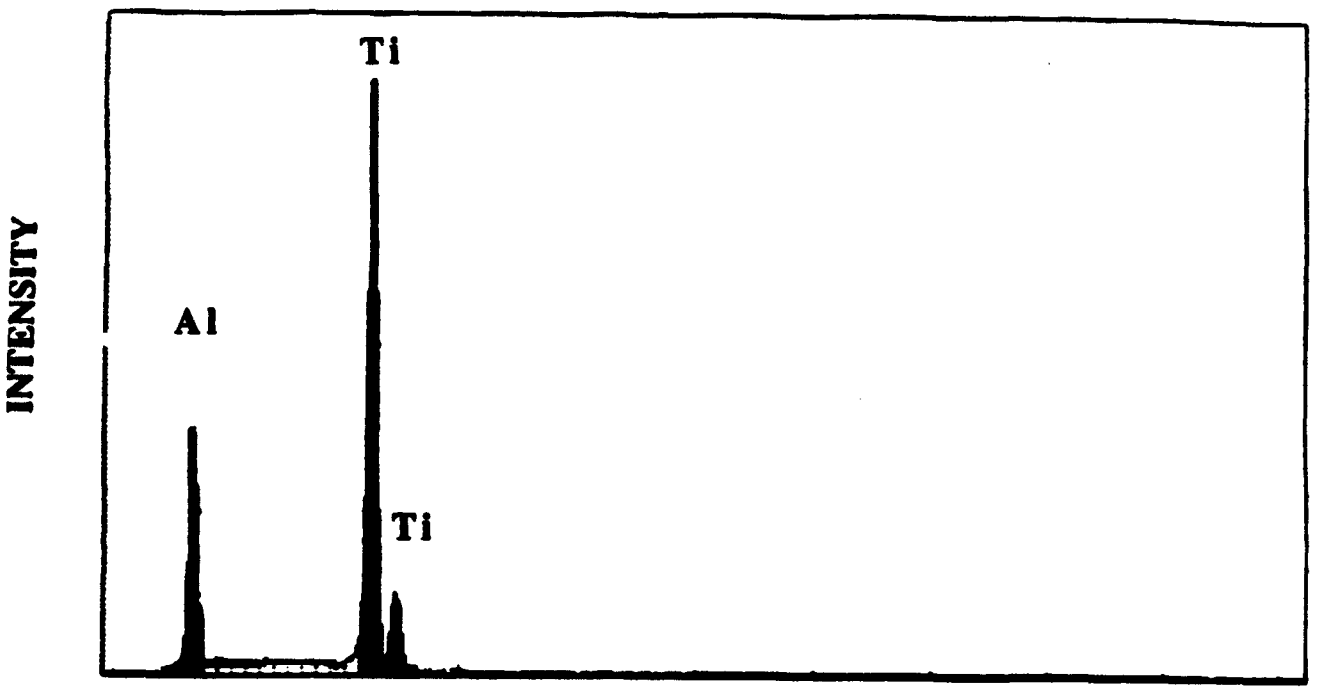

	Atom %
Ti	74.21
Al	25.79

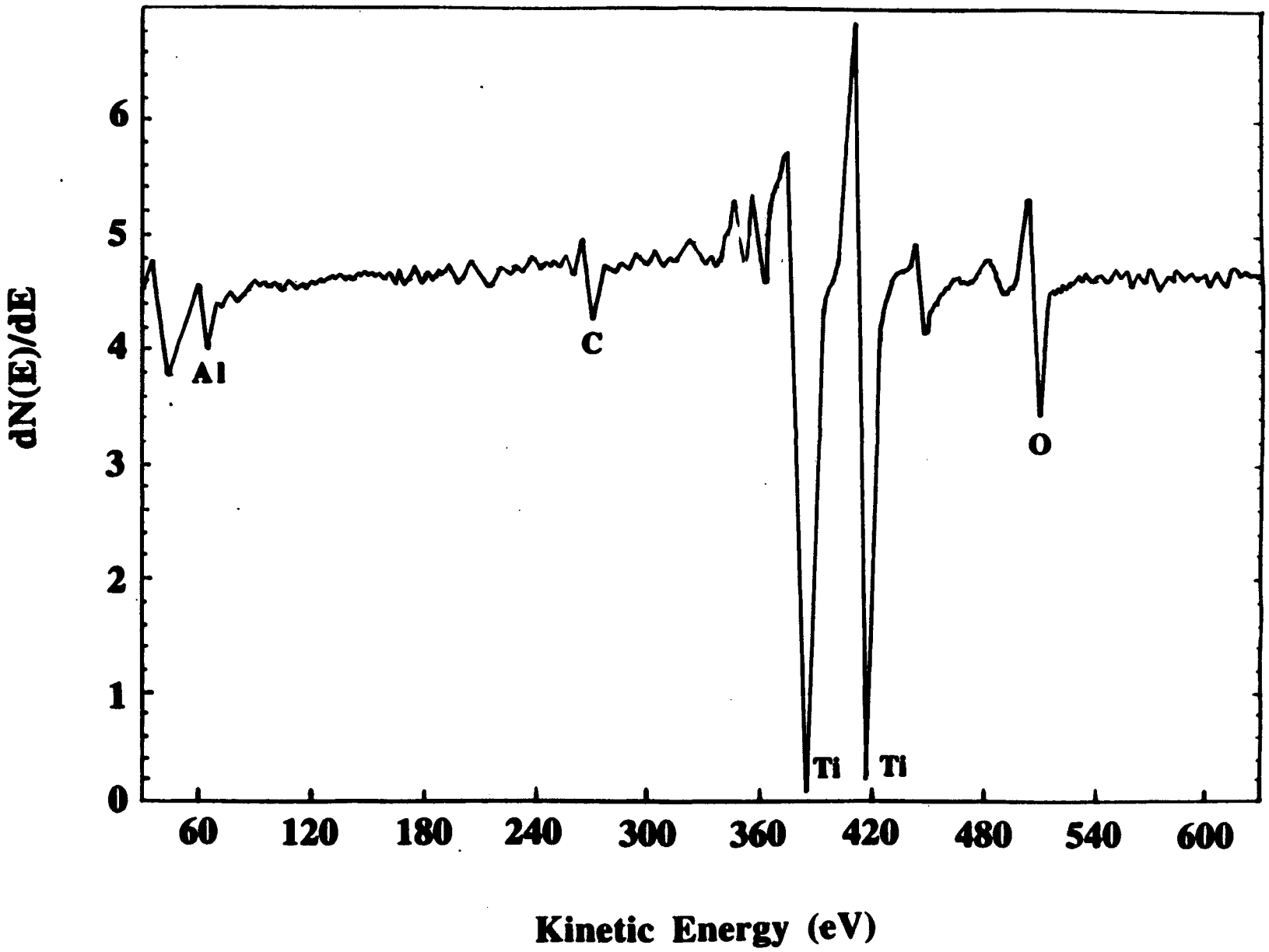
dN(E)/dE
0
1
2
3
4
5
6
Al
C
Ti
Ti
O
60
120
180
240
300
360
420
480
540
600
Kinetic Energy (eV)

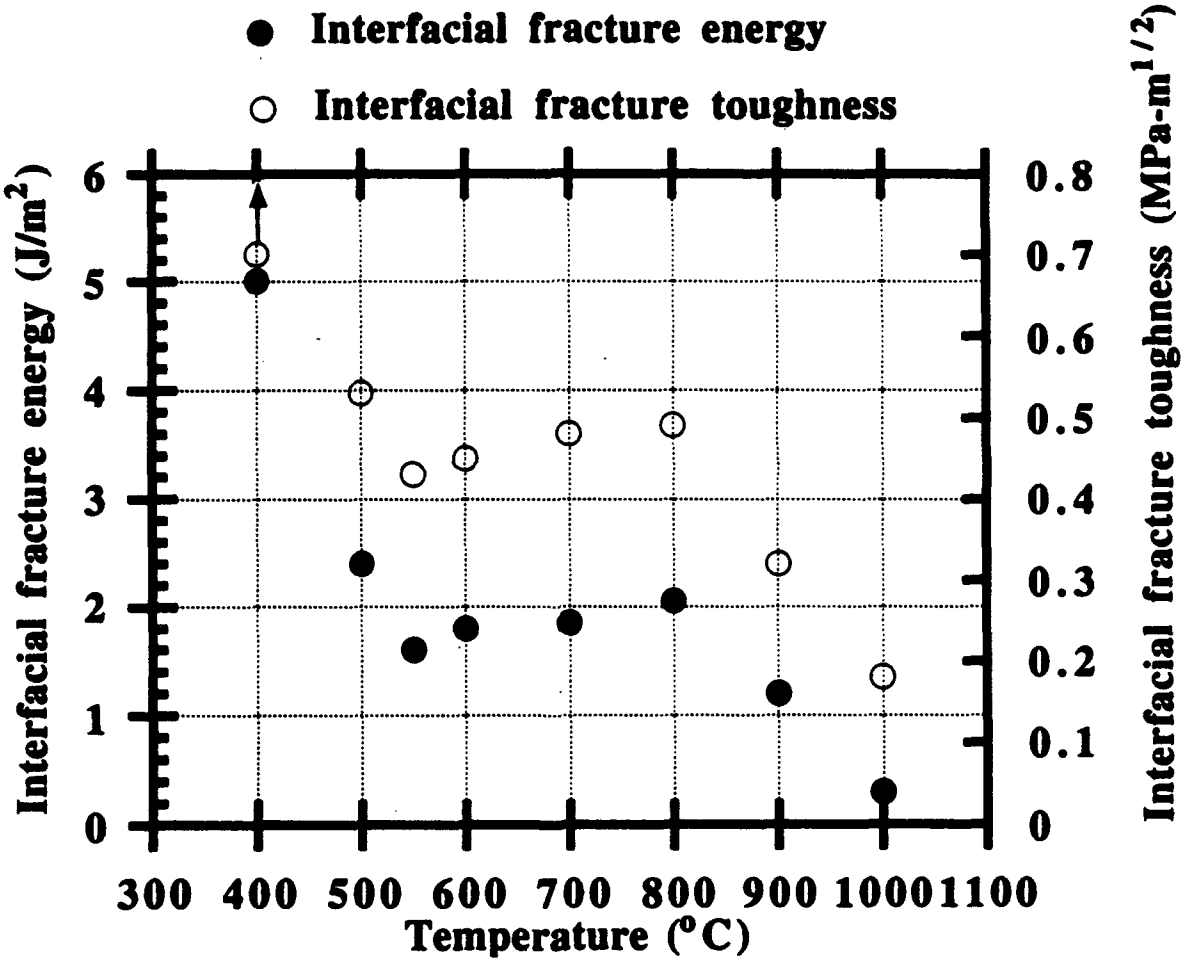
Interfacial fracture energy
Interfacial fracture toughness
Interfacial fracture energy (J/m²)
Interfacial fracture toughness (MPa-m^1/2)
0
1
2
3
4
5
6
0
0.1
0.2
0.3
0.4
0.5
0.6
0.7
0.8
300 400 500 600 700 800 900 1000 1100
Temperature (°C)

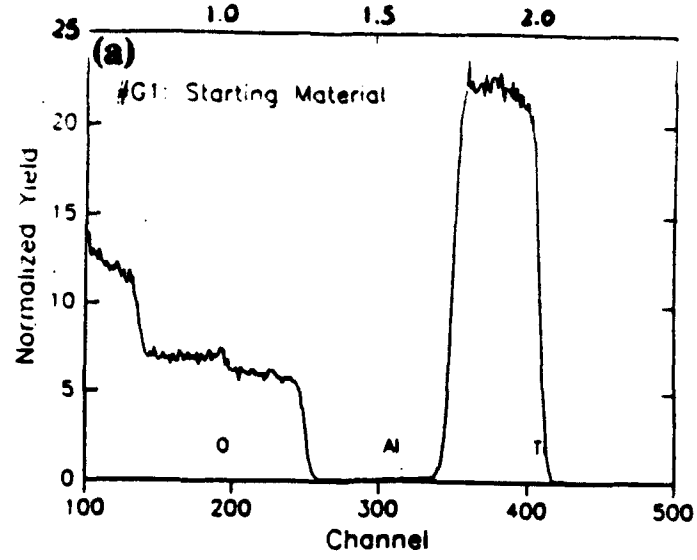
(a)
#G1: Starting Material
Normalized Yield
Channel
O
Al
Ti

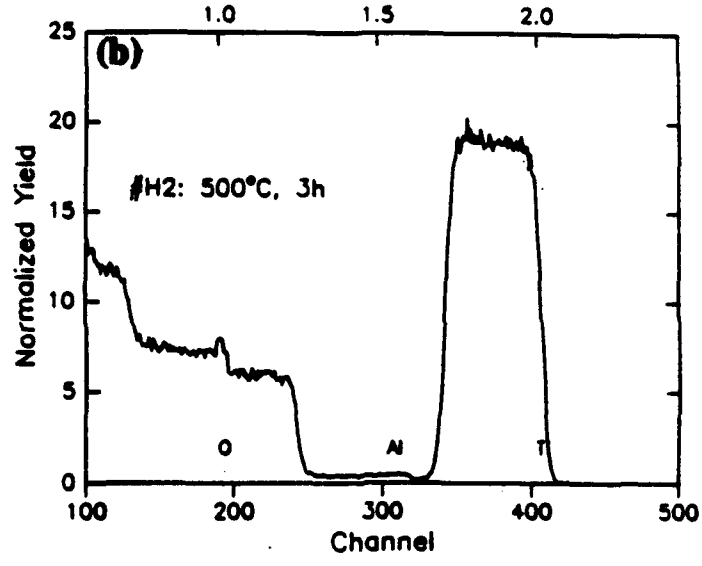
(b)
#H2: 500°C, 3h
Normalized Yield
Channel
O
Al
Ti

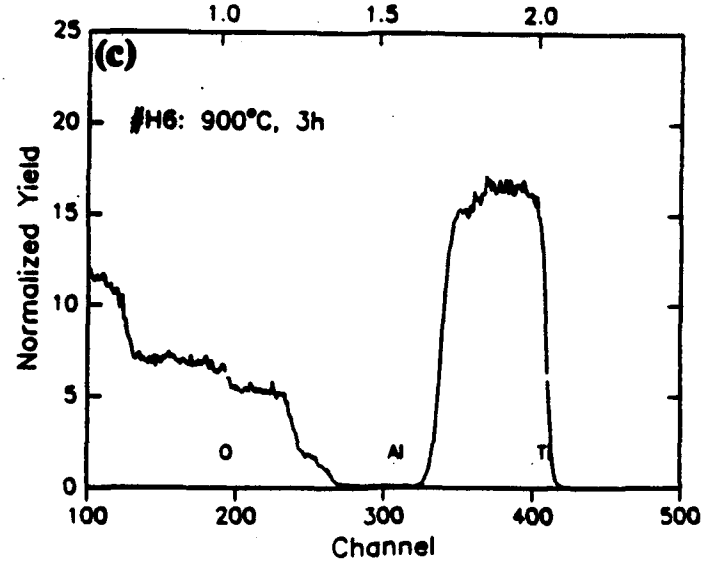
(c)
#H6: 900°C, 3h
Normalized Yield
Channel
O
Al
Ti

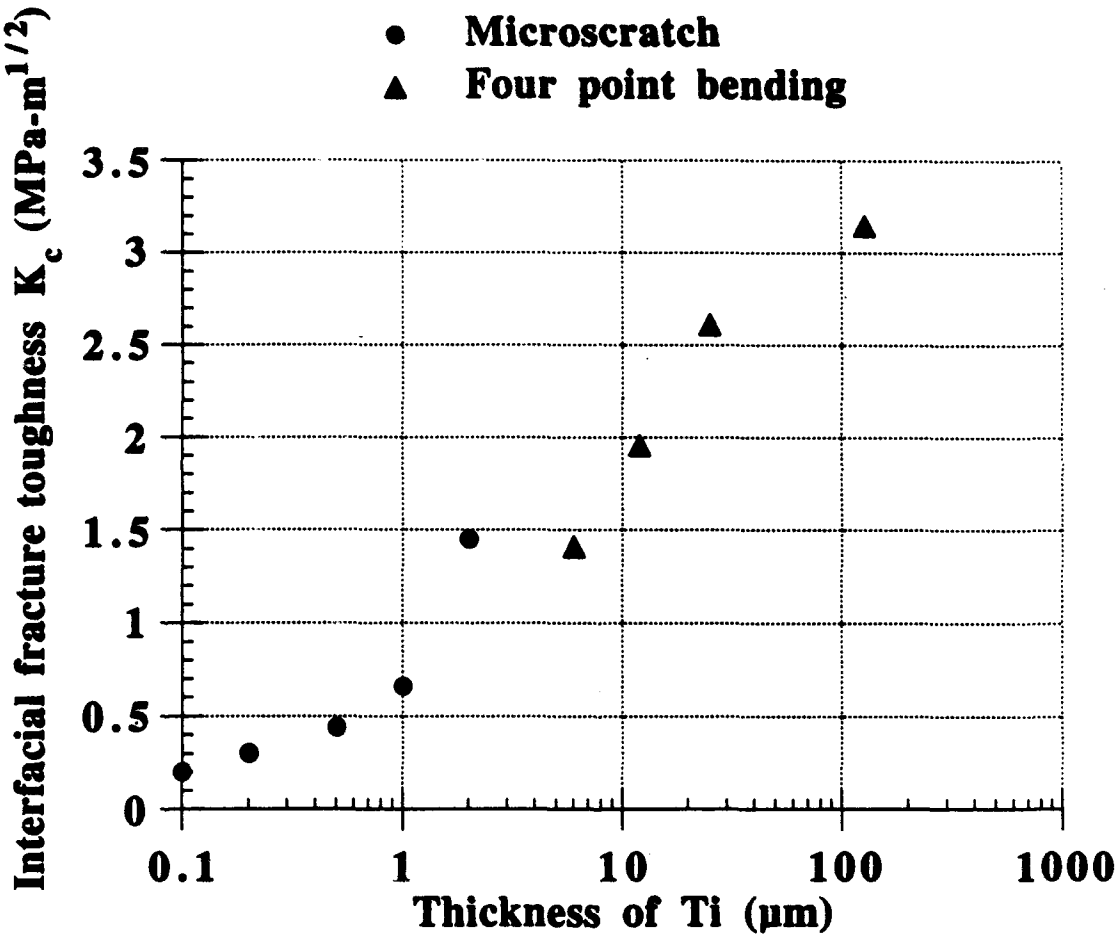
Microscratch
Four point bending
Interfacial fracture toughness K_c (MPa-$m^{1/2}$)
3.5
3
2.5
2
1.5
1
0.5
0
0.1
1
10
100
1000
Thickness of Ti (μm)

Part III:

Effect of a Diffusion Barrier on The Interfacial Chemistry and Mechanical Properties in Ti/Al_2O_3 Composites

H. F. Wang and W .W. Gerberich
Department of Chemical Engineering and Materials Science, University of Minnesota, Minneapolis, Minnesota 55455

ABSTRACT

The interfacial fracture energy of Ti/Al_2O_3 composites was measured with and without a diffusion barrier at different bonding temperatures by using four point bending tests. The diffusion barrier consists of a refractory metal/Y_2O_3 duplex coating. Hot Isostatic Press diffusion bonding was used to prepare sandwich specimens with symmetric precracks for the tests. The interfacial fracture energy was found to increase with increasing bonding temperature up to 950°C. The interfacial fracture energy drops when the bonding temperature was further raised to 1000°C. It was found that the decrease of the interfacial fracture energy is due to the formation of the intermetallic compound, Ti_3Al. By using a diffusion barrier, the interfacial fracture energy decreases from 25.4 to near 0 J/m^2 and 32.9 to 8.7 J/m^2 for applied bonding temperatures of 800 and 900°C, respectively. This is because the barrier reduced the diffusion of Al across the interface and into the Ti, thereby preventing a strong chemical bond. The crack propagation was found to occur at the interface between the Ti and Al_2O_3. By performing fiber pushout tests, the interfacial frictional stress and interfacial fracture energy of the Al_2O_3 fiber reinforced Ti matrix composite were measured to be 312MPa and 0.13 J/m^2, respectively. Note that the interfacial fracture energy measured from the pushout test is smaller than that from the bending tests under the similar processing condition. This is partially due to the surface roughness of the Al_2O_3 fiber being an order of magnitude smaller than that of the Al_2O_3 plate. It is also partially due to the greater plastic energy dissipation in the four-point bending sample compared to the pushout tests, a factor one needs to be aware of when comparing interfacial fracture energies from different specimen types.

1. INTRODUCTION

It is known that the fiber/matrix interface has a dominant effect on the overall mechanical properties of fiber composites[1-4]. Interfacial mechanical properties and chemistry play a very important role in determining the overall mechanical properties of composites. Generally, for a composite with high fracture toughness, it is a prerequisite that the fiber/matrix interface must be "weak" to achieve interfacial debonding and sliding when the composite is under tensile loading[5]. The mechanism of fracture depends on the fracture energy of the constituents, interfacial fracture energy, elastic mismatch and phase angle of loading[6,7].

Moreover, degradation of the interfaces caused by the diffusion of the constituents during the fabrication process at a high bonding temperature and the formation of reaction products is observed in many metal/ceramic systems, like Ti/Al_2O_3 and Ti/SiC[8-11]. In order to maintain the chemical integrity and stability of the metal/ceramic interface, the use of a diffusion barrier is necessary.

The present study focuses on the control of the interfacial mechanical properties in Ti/Al_2O_3 composites with and without a diffusion barrier for different applied bonding temperatures. Systematic measurements of the interfacial fracture energy were accomplished by using four point bending tests of sandwich specimens with symmetric precracks (phase angle of loading $\approx 4/\pi$)[6]. Prior to testing, the composites were bonded at temperatures from 700 to 1000°C. Modification of the interface is also achieved with a diffusion barrier consisting of a refractory metal and Y_2O_3 duplex coating where the Y_2O_3 coating is in contact with the Ti matrix. This diffusion barrier is proprietary to 3M company. The Y_2O_3 is known to be thermodynamically stable with Ti and offers low reactant transport rates[12,13]. Because the Y_2O_3 is very brittle, it is prone to cracking under mechanical and thermal stresses. Therefore, the refractory metal coating is used to reduce the stress at the interface and protect the Y_2O_3. Microstructural and chemical analysis of the sandwich composites with and without the diffusion barrier were performed by using

Scanning Electron Microscopy (SEM), Energy Dispersive X-ray Analysis (EDAX), X-ray mapping, X-ray Photoelectron Spectroscopy (XPS) and X-ray diffraction. Characterization of the as-sputtered diffusion barrier was accomplished. The surface roughness of the Al_2O_3 was measured using a profilometer and an atomic force microscope. To test the diffusion barrier, chemical analysis and fiber pushout tests of an Al_2O_3 fiber reinforced Ti β-21S alloy composite was performed where the composition of the Ti β-21S alloy is Ti-15Mo-3Nb-3Al-0.2Si. The correlation between the interfacial fracture energy and the surface roughness of the Al_2O_3 is also discussed.

2. EXPERIMENTAL

2.1. Sputtering condition

The refractory metal and the Y_2O_3 were deposited separately onto Al_2O_3 substrates by r.f. sputtering. Prior to deposition, the substrates were cleaned with isopropyl alcohol in an ultrasonic cleaner for 20 min. These were then placed in the sputtering chamber. After evacuating the chamber to a background pressure < 5 x 10^{-7} Torr, sputtering was performed at an Ar pressure of 10 mTorr, with a power density of 16 W/cm^2 for the refractory metal and 14.8 W/cm^2 for the Y_2O_3. The substrate temperature during deposition was not more than 80 °C. During deposition, with a deposition rate of about 70Å/min for 1 hr, the distance between the target and the substrate was maintained at 75mm. This produced a final thickness of each coating of 0.4 μm.

2.2. Sample preparation conditions

The test specimen which served as a model system to evaluate the interfacial fracture energy consists of a bimaterial beam with symmetric precracks, as shown in Fig.1. To make sandwich specimens without the diffusion barrier for the four point bending tests, they were prepared as follows: thin foils of Ti (99.8% pure) and Al_2O_3 plates were immersed in isopropyl alcohol for 10 min and then cleaned in an ultrasonic

cleaner for 20 min. The thickness of the Ti foils is 25 μm. They were sandwiched with a 3mm gap between the two foils to form a precrack, wrapped with Ta foils and encapsulated in glass containers evacuated to 10^{-6} torr. They were then Hot Isostatic Press (HIP) bonded in an Ar gas atmosphere. Specimens were first heated to the softening point of the glass under a pressure of 1.75 MPa for 30 min and then pressure and temperature were simultaneously raised to 7 MPa and a fixed temperature which ranged from 700°C to 1000°C. The sandwich specimens with the diffusion barrier were also bonded with applied bonding temperatures of 800°C and 900°C. The bonding time was fixed at 1hr. After HIPing, a notch was cut in the sandwich specimen from the Al_2O_3 side with a low speed diamond saw. Because of the gap between the foils, this forms a well defined precrack.

The specimens were placed in a four point bending fixture mounted on an MTS machine with load and displacement being recorded with a chart recorder during the test. A critical load drop marks the propagation of a crack along the interface between Ti and Al_2O_3. This critical load was used to calculate the interfacial fracture toughness. The details of the calculation are described elsewhere[14]. After the four point bending tests were completed, the specimens were cut perpendicular to the bonding interface with a low speed diamond saw. The exposed cross section was then polished to facilitate microstructural observation and chemical analysis.

2.3. Instruments for microstructural and chemical analysis

Before the HIPing process, the Y_2O_3 coatings were characterized by a Perkin-Elmer PHI 5400 ESCA system with a background pressure of less than $5x10^{-10}$ for X-ray Photoelectron Spectroscopy (XPS) analysis. The resolution is 0.2 eV. A surface layer of 100 Å was removed by sputter etching before the analysis. A Digital Instruments Nanoscope III atomic force microscope was used for the surface roughness measurement with lateral resolution 5 Å and vertical resolution 1 Å. Microstructural observations and

chemical analyses of the sandwich composites after the HIPing were conducted by Scanning Electron Microscopy (SEM), Energy Dispersive X-ray Analysis (EDAX), X-ray mapping by using a JOEL 840 Scanning Electron Microscope at 20 KV. X-ray diffraction was performed using a Siemens D-500 with a Cu Kα radiation source.

3. RESULTS AND DISCUSSION

3.1 Criterion for interfacial debonding

As shown in Fig. 2, there is a matrix crack which propagates and meets the fiber. Whether the crack propagates across the fiber or along the interface is determined by the critical value G_{ic}/G_f, where G_{ic} is the critical mixed mode interfacial fracture energy (phase angle of loading $\approx 4/\pi$) for fiber debonding and G_f is the fracture energy of the fiber (40 J/m^2 for Al_2O_3). The critical value is dependent on the elastic mismatch α.

$$\alpha = \frac{\mu_1(1-\nu_2)-\mu_2(1-\nu_1)}{\mu_1(1-\nu_2)+\mu_2(1-\nu_1)}$$

with μ being the shear modulus, ν Poisson's ratio and the subscript 1 and 2 referring to materials 1 and 2 respectively.

Plane strain calculation shows that interfacial debonding occurs provided G_i/G_f is smaller than G_{ic}/G_f where G_i is the measured interfacial fracture energy[1]. The elastic mismatch α for Ti/Al_2O_3 is 0.5, which gives the ratio $G_{ic}/G_f = 0.45$ from Fig.2. That means G_i must be smaller than G_{ic}(=18 J/m^2) to meet the prerequisite for interfacial debonding for Al_2O_3 fiber reinforced Ti matrix composites.

3.2. Characterization of the Y_2O_3 coating and the coated Al_2O_3 fiber

The characterization of the Y_2O_3 coating is shown in Fig.3. After the deconvolution, there is a main peak with a binding energy of 156.6 eV. This value is close to the Y^{3+} $3d^{5/2}$ peak in Y_2O_3 which is 156.4 eV[15]. That means a pure Y_2O_3 oxide

layer was formed on the Al_2O_3 after the sputtering process. This Y_2O_3 coating has also been confirmed by using X-ray diffraction which shows a strong Y_2O_3 (101) peak. The root-mean-square surface roughness of the diffusion barrier coated Al_2O_3 fiber is 18.8 nm which was measured using an atomic force microscope.

3.3. Analysis of Ti/Al_2O_3 sandwich composites

By using a profilometer, the root-mean-square surface roughness of the as-received Al_2O_3 plate is 0.3 μm. The interfacial fracture energy was measured at different applied bonding temperatures for a 25 μm thickness Ti interlayer. The relationship between interfacial fracture energy of the Ti/Al_2O_3 composites and bonding temperature is shown in Fig.4. The interfacial fracture energy of the composite without the diffusion barrier increases from near 0 to 34.1 J/m^2 as the bonding temperature increases from 700 to 950°C. It appeared that there was no bonding strength between the Ti and Al_2O_3 when the applied bonding temperature is 700°C. This is because a thin native Ti oxide layer formed on the Ti surface before the diffusion bonding process which prevents the diffusion of the constituent atoms to form a chemical bonding during the HIPing. Alternatively, there could have been some weak bonding which failed on cooling due to thermal expansion mismatch stress. At higher temperature, the Ti is softer which allows the asperities of the Al_2O_3 surface to break the Ti oxide and come in contact with the Ti metal[16-18]. Thus, the Al ions can diffuse into Ti metal to form a strong chemical bond which results in higher interfacial fracture energy. However, the interfacial fracture energy drops to 16.9 J/m^2 when the bonding temperature was raised to 1000°C. The SEM cross-sectional view of a sandwich specimen which was bonded at 1000°C is shown in Fig. 5(a). A reaction layer is found to exist between Ti and Al_2O_3. The backscattered electron image shows a slight contrast difference between the reaction layer and the Ti (Fig. 5(b)). From the X-ray map, the diffusion of Al into Ti is seen to be much faster than that of Ti into Al_2O_3. The diffusion distance of Al is more than 5μm. The composition of the

reaction product at the interface was analyzed by using EDAX with the semi-quantitative data being shown in Fig. 6. From the measured atomic % of Ti and Al, the reaction layer between Ti and Al_2O_3 is identified as Ti_3Al. The XPS analysis of the reaction product shows the same result. Because the Ti_3Al intermetallic compound is very brittle[19,20], it will reduce the fracture energy of the Ti/Al_2O_3 interface. It is expected that when the bonding temperature is 1000°C, a great deal of Ti_3Al is produced which will decrease the interfacial fracture energy of Ti/Al_2O_3 composites. The interfacial fracture energy of the composites with the refractory metal/ Y_2O_3 diffusion barrier was found to be near 0 and 8.7 J/m^2 at applied bonding temperatures of 800 and 900°C respectively. These values are much smaller than that without the diffusion barrier at the same bonding temperature. The diffusion barrier significantly reduces the interfacial fracture energy from 25.4 to near 0 J/m^2 at 800°C and 32.9 to 8.7J/m^2 at 900°C. The interfacial fracture energy of the composites with the diffusion barrier is seen to meet the basic requirement for interfacial debonding (smaller than G_{ic}=18J/m^2). By performing the X-ray mapping of the sandwich composite with the diffusion barrier, the effect of the diffusion barrier is seen to decrease the diffusion of the Al ions across the interface and into the Ti to from the chemical bonding. Therefore, it reduces the interfacial fracture energy. There is some interdiffusion of Al, Ti, the refractory metal and Y during the HIPing which produces the diffuse interfaces in the Ti/Al_2O_3 system.

Typical cross-section view of the composite without the diffusion barrier before and after the four point bending tests is shown in Fig. 7. It is clearly seen that the failure process occurred at the interface between the Ti and Al_2O_3. The SEM observation of the Ti and Al_2O_3 fracture surface after the four point bending also confirms an interfacial fracture process. For the sandwich composite without the diffusion barrier and bonded at 900°C, many Ti_3Al nodules were found on the Ti and Al_2O_3 fracture surface, as shown in Fig.8. The fracture surface of the composite with the diffusion barrier shows a different feature (Fig. 9). A thin layer of the diffusion barrier is seen on the Ti and Al_2O_3 fracture surface.

EDAX analysis of the Ti fracture surface shows a strong Ti peak, a weak refractory metal peak, a weak Y peak and a very weak Al peak . The presence of the Al peak in the spectrum of the Ti fracture surface means that there is still some diffusion of the Al into the diffusion barrier during the HIPing process. For the Al_2O_3 fracture surface, there is a strong Al peak, a weak refractory metal peak and a weak Y peak. From these results, it is seen that the crack propagates in the diffusion barrier between the Ti and Al_2O_3 and it does not follow a well defined interface such as Ti/Y_2O_3, Y_2O_3/refractory metal or refractory metal/Al_2O_3.

2.4. Analysis of an Al_2O_3 fiber reinforced β-21S Ti matrix composite

To evaluate the chemical stability of the refractory metal/Y_2O_3 duplex diffusion barrier in a practical application, an Al_2O_3 fiber reinforced β-21S Ti matrix composite prepared by the HIPing at 900°C was analyzed with SEM and X-ray mapping, as shown in Fig. 10. The interfiber spacing in the composite is about 10 μm. The fiber (diameter =10 μm) is uniformly coated with the refractory metal/Y_2O_3 duplex diffusion barrier. From the Al x-ray mapping (Fig 10(a)), it is shown that the diffusion distance of the Al into the Ti is about 0.5-0.7 μm. This is considerably smaller than that without the diffusion barrier which is 5 μm under similar processing conditions. From the Ti X-ray mapping, the diffusion of Ti into Al_2O_3 is very limited. There is a small amount of diffusion of the refractory metal and Y (Fig. 10(c),(d)), although they mostly remain at the fiber/matrix interface.

The refractory metal /Y_2O_3 duplex diffusion barrier reduces the chemical reaction between Ti and Al_2O_3 and prevents the formation of the Ti_3Al intermetallic compound. Therefore, it maintains the chemical stability and integrity of the Ti/Al_2O_3 interface. Modification of the interfacial mechanical properties with this diffusion barrier seems feasible.

The interfacial frictional stress and interfacial fracture energy in the Al_2O_3 fiber reinforced β-21S Ti matrix composite were measured by using the fiber pushout tests. After the pushout test, a micrograph of the top and bottom of the composite after the pushout tests is shown in Fig.11. The interfacial frictional stress and interfacial fracture energy were calculated to be 312 MPa and 0.13 J/m^2 respectively. The details of the experimental procedures and the calculation are described elsewhere[21]. The measured interfacial fracture energy is smaller than the 8.7 J/m^2 value measured for similar processing conditions using the four-point bending tests. This is partially due to the difference in the surface roughness of the Al_2O_3 fiber (18.8nm) for the fiber pushout tests and that of the Al_2O_3 plates (0.3μm) for the bending tests. It is known that the surface roughness induces crack tip shielding by means of friction and locking during the crack propagation process and thereby increases the interfacial fracture energy[22]. It is also partially due to the greater plastic energy dissipation in the four-point bending sample compared to the pushout tests, a factor one needs to be aware of when comparing interfacial fracture energies from different specimen types. The interfacial fracture energy measured from the fiber pushout tests meets the prerequisite for interfacial debonding in fiber composites.

4. CONCLUSIONS

The interfacial fracture energy increases from near 0 to 34.1 J/m^2 as the applied bonding temperature is changed from 700 to 950°C. It then decreases when the temperature is further raised to 1000°C. The degradation of the composite at 1000°C is due to the formation of the intermetallic compound, Ti_3Al. With a refractory metal/Y_2O_3 diffusion barrier, the interfacial fracture energy drops from 25.4 to near 0 J/m^2 and 32.9 to 8.7 J/m^2 for bonding temperatures of 800 and 900°C respectively. The fracture process occurs at the Ti/Al_2O_3 interface. By analyzing the Al_2O_3 fiber reinforced Ti matrix composites, it is seen that the diffusion barrier reduces the diffusion of the Al into Ti.

This decreases the degree of the chemical bonding and prevents the formation of the Ti_3Al. Thus, the chemical integrity and stability of the Ti/Al_2O_3 interface can be maintained throughout the HIPing process. This provides a useful metal/ceramic duplex coating for the Al_2O_3 fiber reinforced Ti matrix composites for high fracture toughness. The interfacial frictional stress and interfacial fracture energy of the fiber composite were measured to be 312 MPa and 0.13 J/m^2 respectively. The difference in the interfacial fracture energy measured from the bending tests and the pushout tests is due to the difference in the measured surface roughness of the Al_2O_3 fiber and Al_2O_3 plate and the volume of metal undergoing plastic energy dissipation.

ACKNOWLEDGMENTS

This research was supported by 3M/DARPA/ONR Metal Matrix Composite Model Factory Program under subcontract No. GS 01080 - KAS and ONR N/N00014-92-J-1962. The authors wish to acknowledge Dr. H.E. Deve and Dr. R.R. Kieschke for providing the fiber composites, Mr. C.J. Skowronek and Mr. C.L. Lin for the sample preparation, Mr. D.Z. Liu for surface analysis and Dr. J. C. Nelson for helpful discussions.

REFERENCES

1. A.G. Evans, F.W. Zok and J. Davis, *Composite Sci. Technol.*, 1991, vol. 42, pp. 3.
2. M.D. Thouless and A.G. Evans, *Scrip. Metal. et. Mater.*, 1990, vol. 24, pp. 1507.
3. H.M. Jensen. *Acta. Metall. Mater.*, 1990, vol. 38, pp. 2637..
4. Y.M. Yang, S.M. Jeng and C.J. Yang, *Mater. Sci. Eng.*, 1991, vol. A138, pp. 155.
5. A.G.Evans, *Mater. Sci. Eng.*, 1991, vol. A143, pp. 63.
6. A.G. Evans, M. Ruhle , B.J. Dalgleish and P.G. Charalambides, *Mater. Sci. Eng.*, 1990, vol. A126, pp. 53.
7. M.Y. He, A. Bartlett, A.G. Evans and J.W. Hutchinson, *J. Am. Ceram. Soc.*, 1991, vol. 74, pp. 767.
8. X.L. Li, R. Hillel, F. Teyssandier, S.K. Choi and F.J.J. Van Loo, *Acta. Met. Mater.*, 1992, vol. 40, pp. 3149.
9. M.B. Chamberlain, *J. Vac. Sci. Technol.*, 1978, vol. A15, pp. 240.
10. C. Jones, C.J. Kiely and S.S. Wang, *J. Mater. Res.*, 1989, vol. 4, pp. 327.
11. J.M. Yang and S.M. Jeng, *Scripta Metall.*, 1989, vol. 23, pp. 1159.
12. R.R. Kieschke and T.W. Clyne, *Mater. Sci. Eng.*, 1991, vol. A135, pp. 145.
13. R.R. Kieschke, C.M. Warwick and T.W. Clyne, *Acta. Met. Mater.*, 1991, vol. 39, pp. 445.
14. H.F. Wang, C.J.Skowronek and W.W. Gerberich, *Acta. Met. Mater.*, in press
15. C.D. Wagner, W.M. Riggs, L.E. Davis, J.F. Moulder and G.E. Muilenberg: *Handbook of X-ray Photoelectron Spectroscopy* , Perkin-Elmer Corporation, 1978, pp. 98.
16. J. T. Klomp, A.J. C. Van de Ven, *J. Mater. Sci.*, 1980, vol. 15, pp. 2483.
17. B. Derby : *Joining of Ceramics* , M.G. Nichloas, eds., Chapman and Hill, 1990, Chapter 6.
18. O.M. Akselsen, *J. Mater. Sci.*, 1992, vol. 27. pp. 569.
19. H.A. Lipsitt, D. Shechtman and R.E. Schafrik, *Metall. Trans.*, 1980, vol. 11A,

pp. 1370.

20. H.T. Kestner-Weykamp, C.H. Ward, T.F. Broderick and M.J. Kaufman, *Scripta Met.*, 1989, vol. 23, pp. 1697.

21. H.F. Wang, J.C. Nelson, W.W. Gerberich and H.E. Deve, unpublished research.

22. A.G. Evans and J.W. Hutchinson, *Acta. Metall. Mater.*, 1989, vol. 37, pp. 909.

LIST OF FIGURES

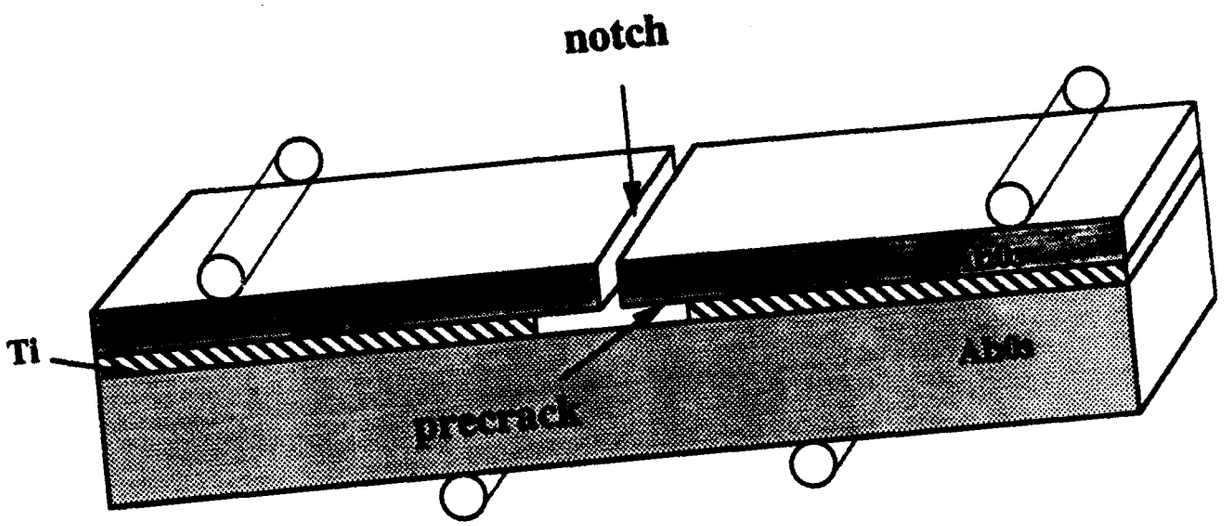
notch
Ti
precrack
Al2O3

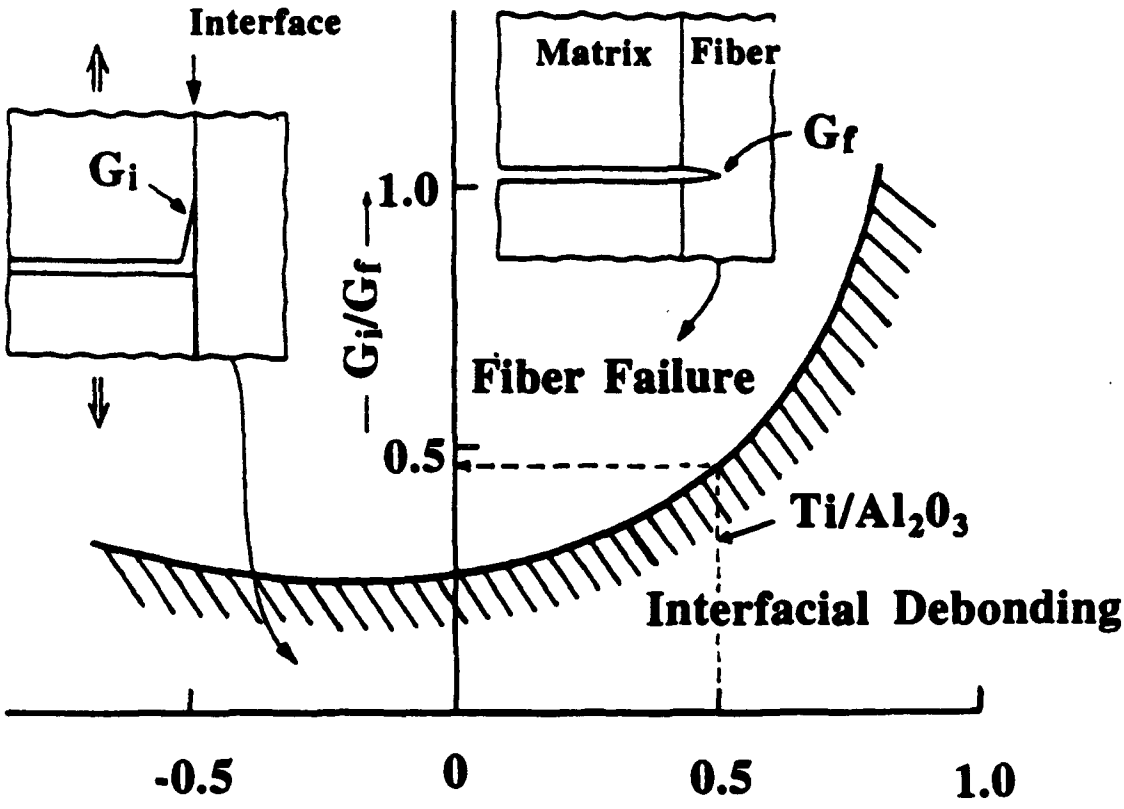
Interface
Matrix
Fiber
G_i
G_f
1.0
G_i/G_f
Fiber Failure
0.5
Ti/Al_2O_3
Interfacial Debonding
-0.5
0
0.5
1.0
Elastic Mismatch, α

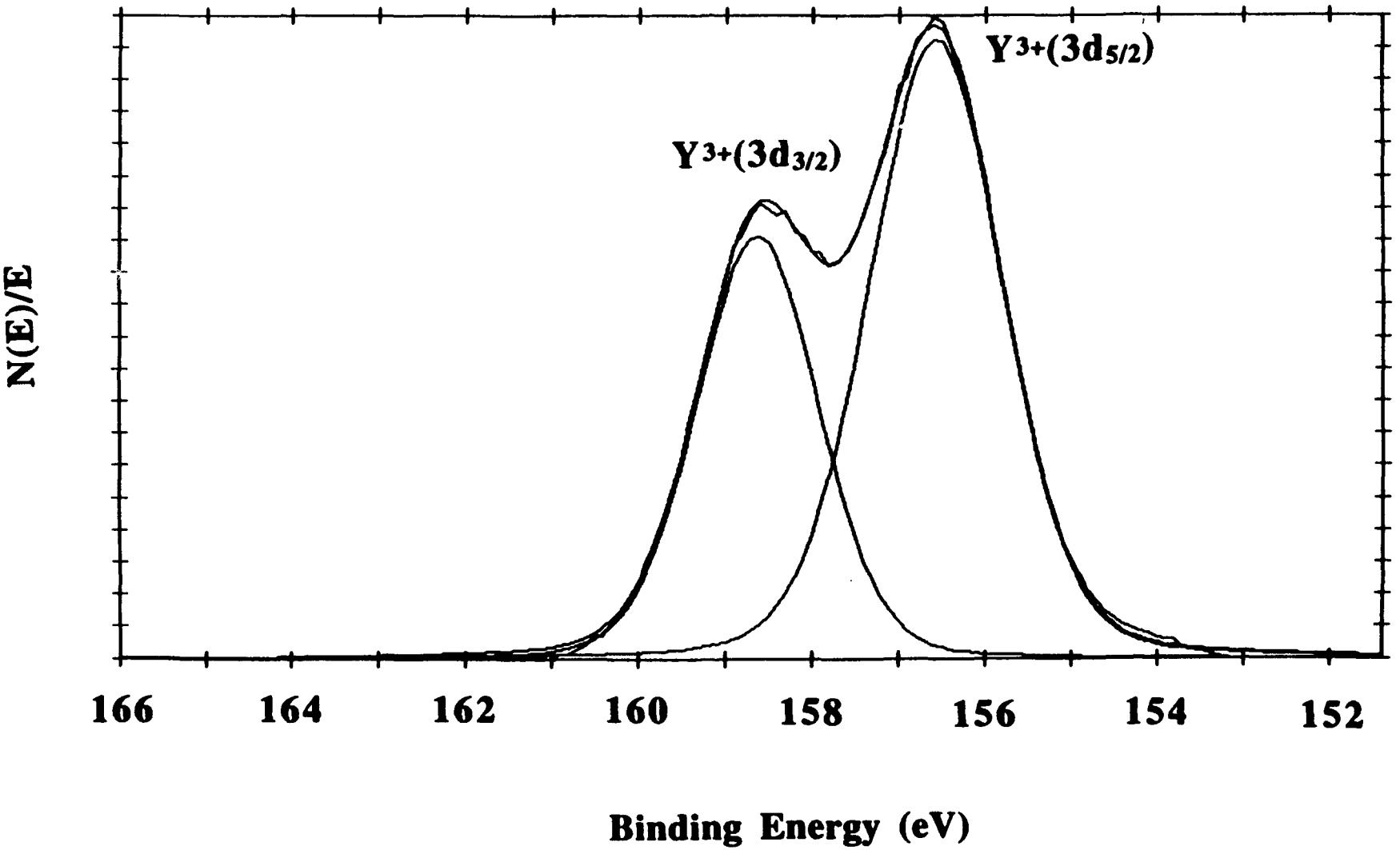
Y3+(3d5/2)
Y3+(3d3/2)
N(E)/E
166
164
162
160
158
156
154
152
Binding Energy (eV)

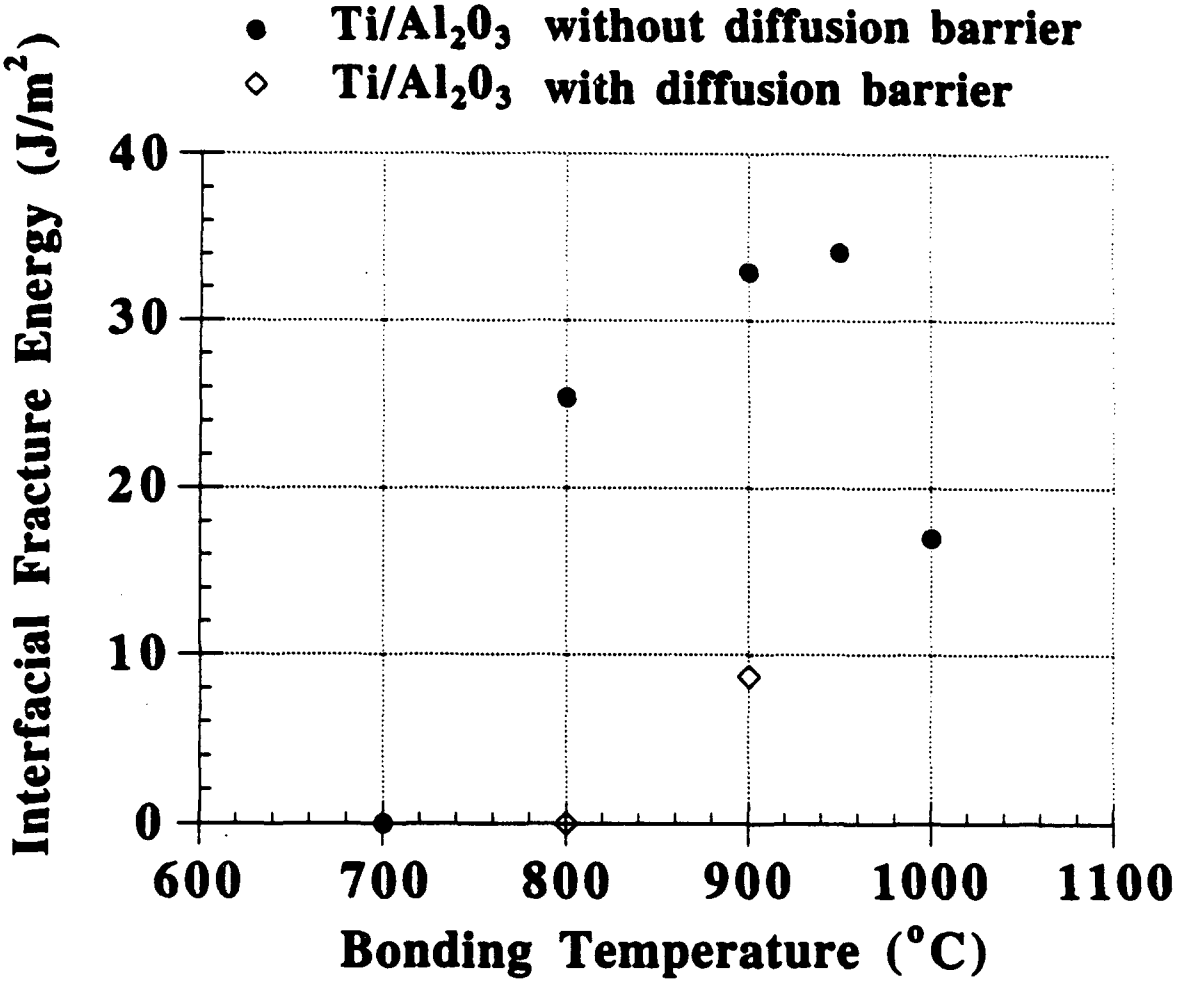
● Ti/Al2O3 without diffusion barrier
◇ Ti/Al2O3 with diffusion barrier
Interfacial Fracture Energy (J/m2)
40
30
20
10
0
600
700
800
900
1000
1100
Bonding Temperature (°C)

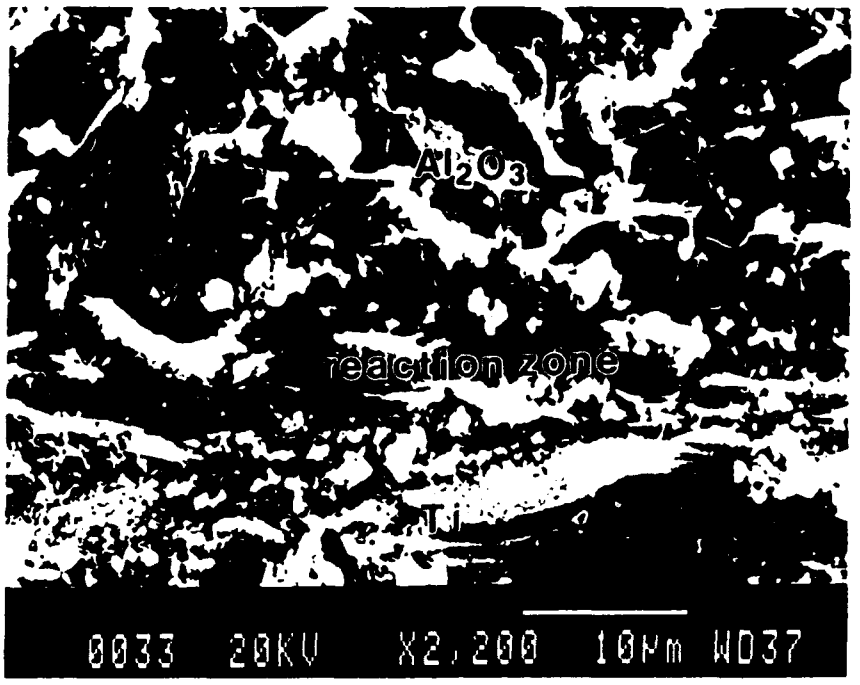
Al_2O_3
reaction zone
Ti
0033 20KV X2,200 10μm WD37

(a)

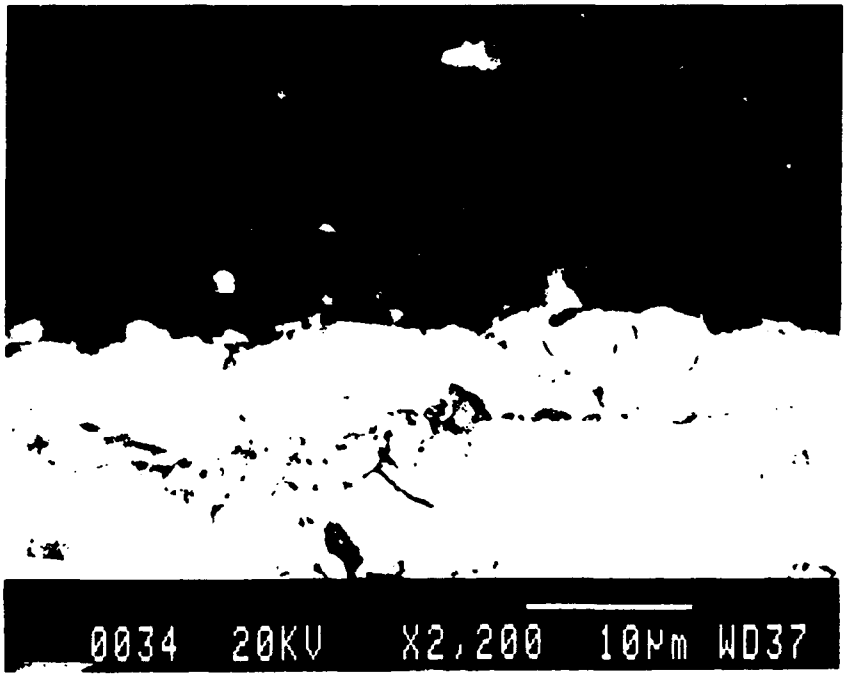
0034 20KV X2,200 10μm WD37

(b)

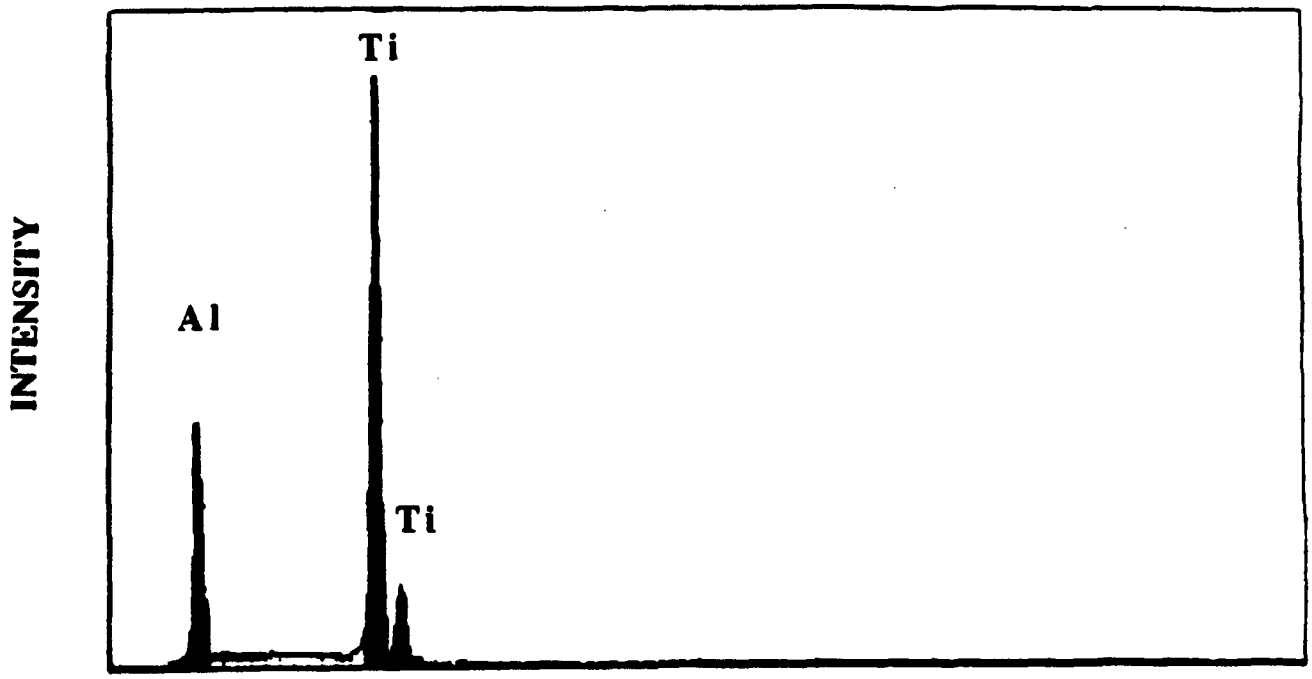

	Atom %
Ti	74.21
Al	25.79

⇒ Ti_3Al

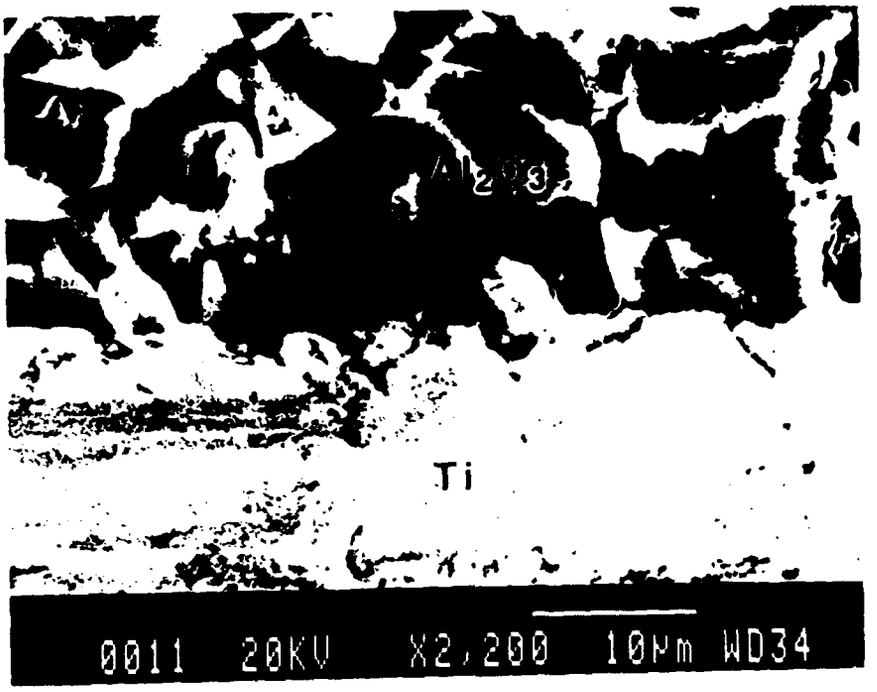

(a)

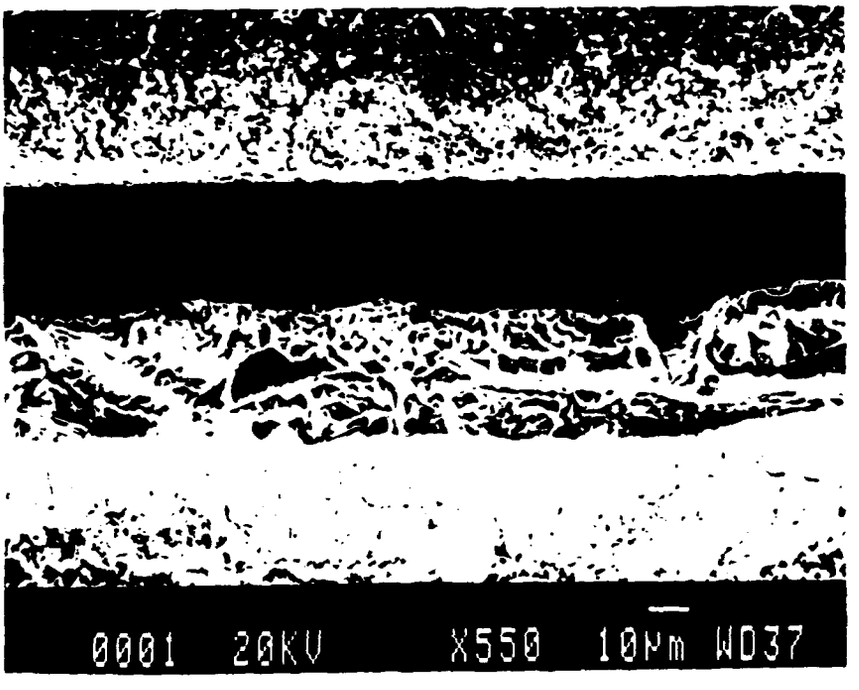

(b)

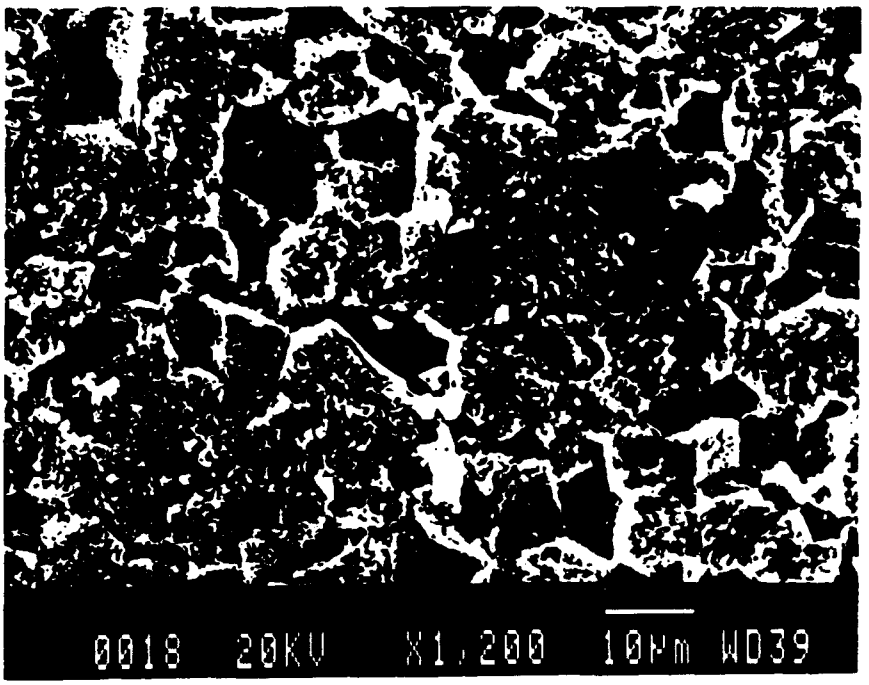

(a)

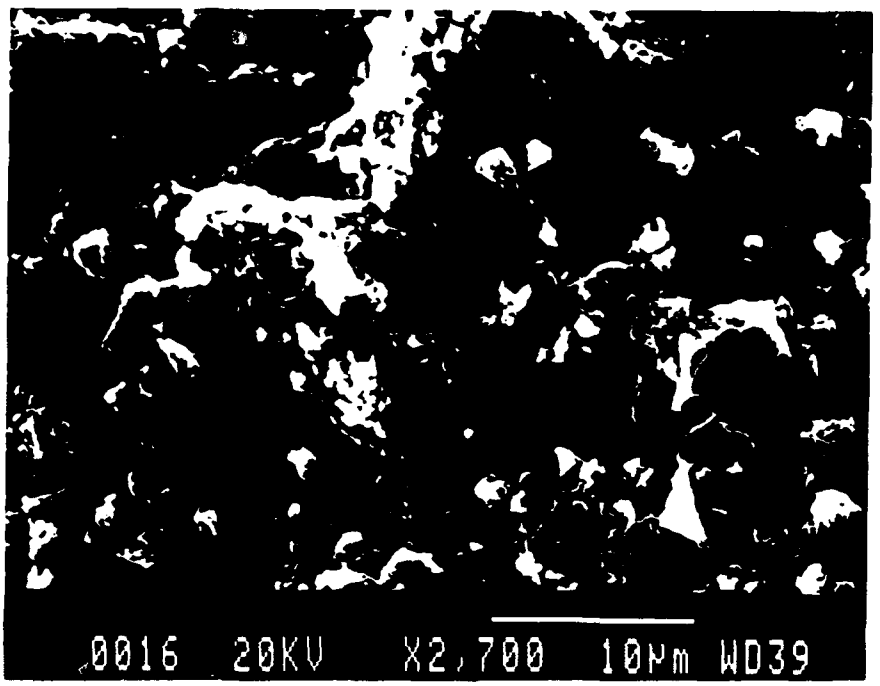

(b)

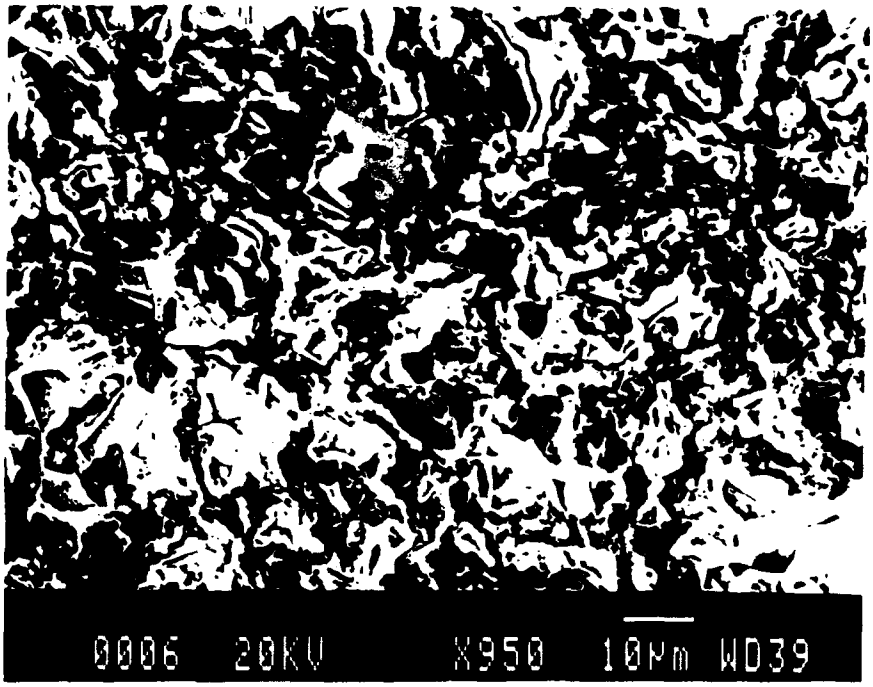

(a)

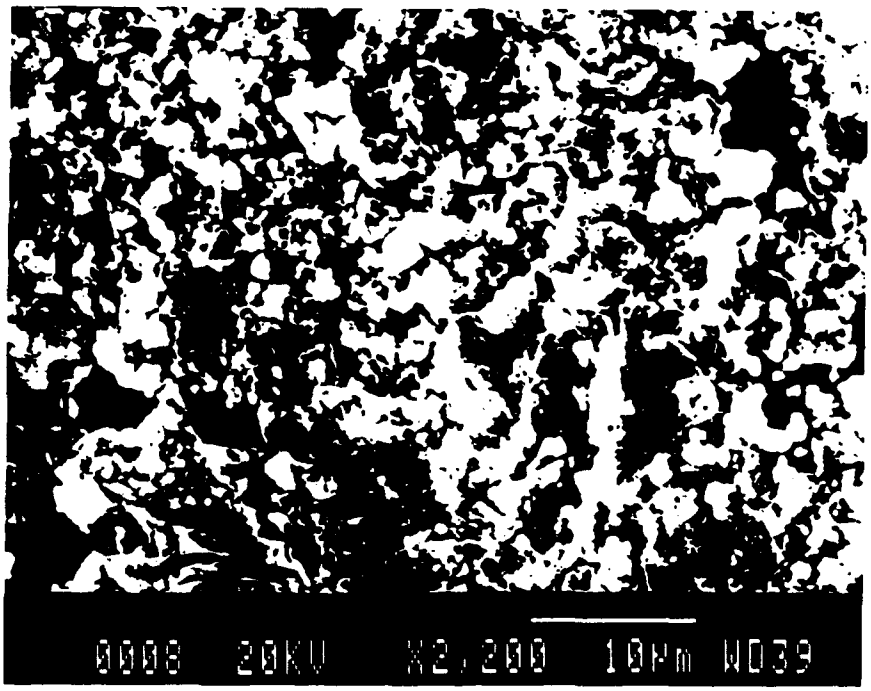

(b)

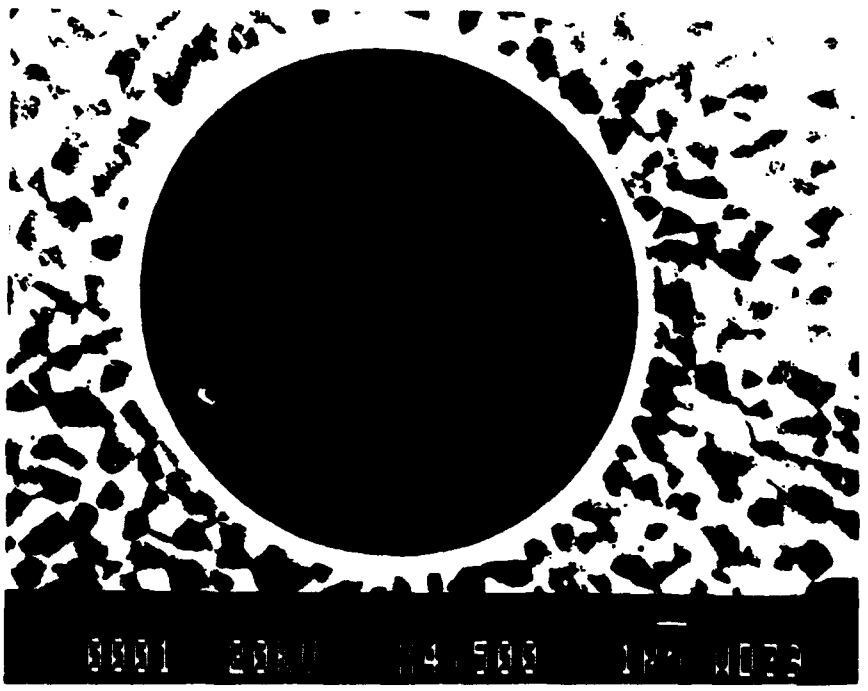

(a)

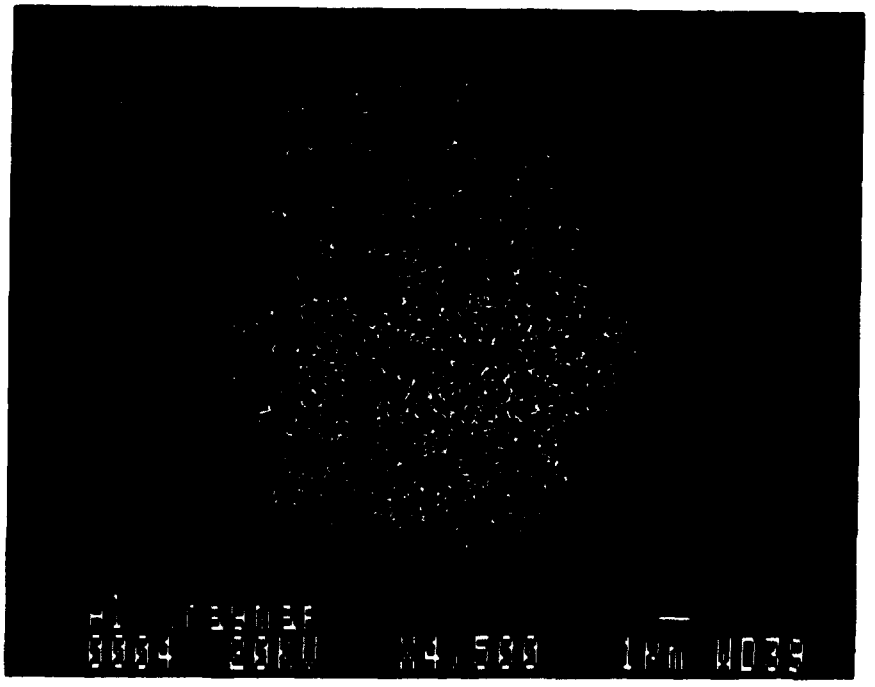

(b)

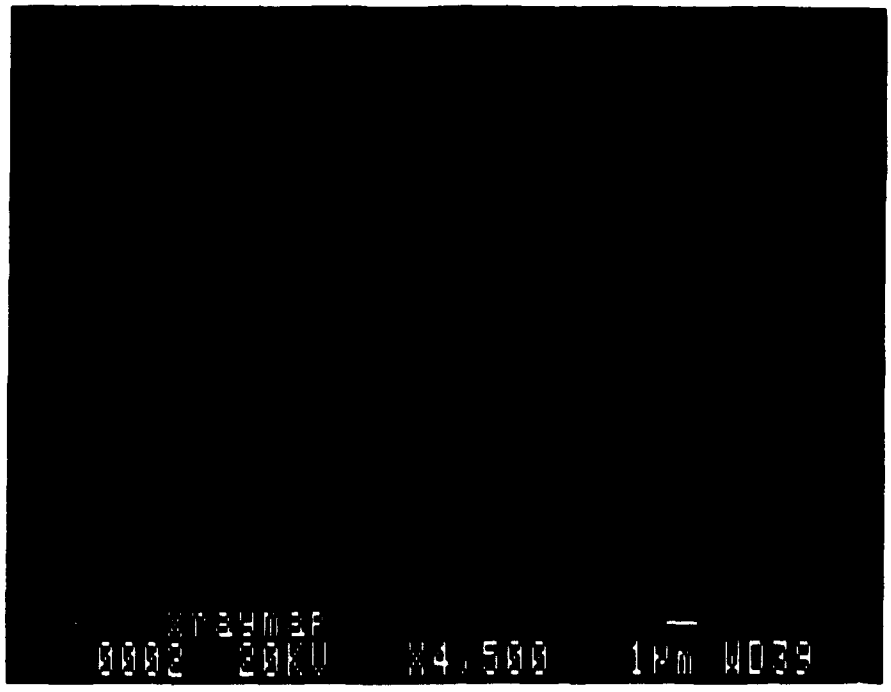

(c)

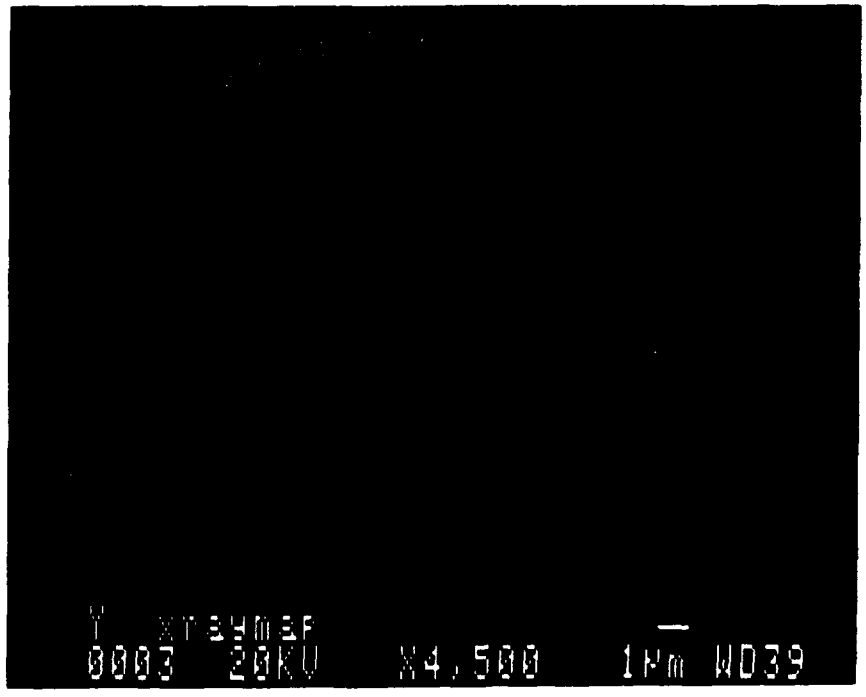

(d)

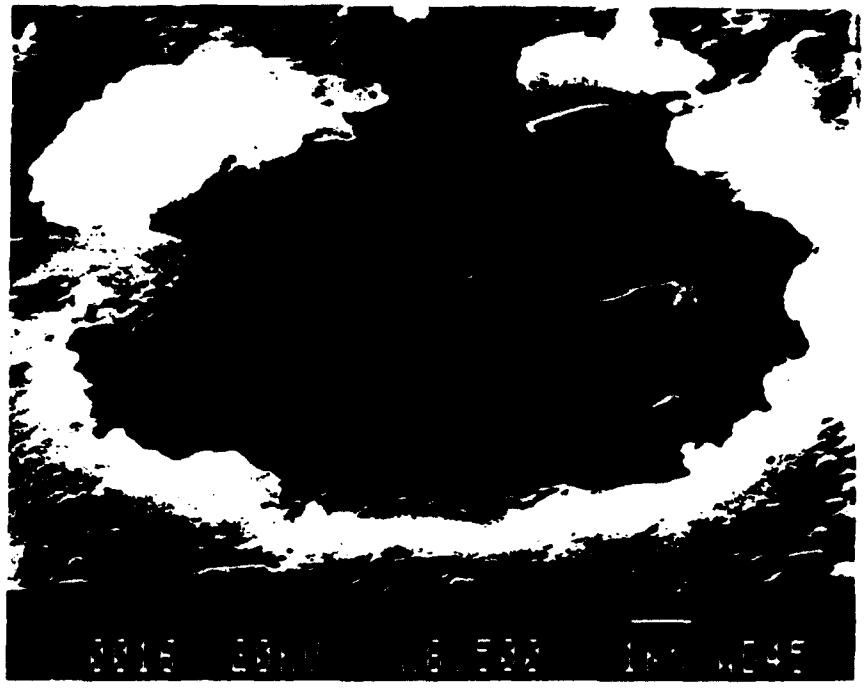

(a)

(b)